
Electronic Thesis and Dissertation Repository

7-29-2016 12:00 AM

Comprehensive Topological, Geometric, And Hemodynamic Analysis Of The Rat Gluteus Maximus Arteriolar Networks

Mohammed K. Al Tarhuni
The University of Western Ontario

Supervisor

Dwayne N. Jackson
The University of Western Ontario Joint Supervisor

Daniel Goldman
The University of Western Ontario

Graduate Program in Medical Biophysics

A thesis submitted in partial fulfillment of the requirements for the degree in Master of Science

© Mohammed K. Al Tarhuni 2016

Follow this and additional works at: <https://ir.lib.uwo.ca/etd>



Part of the [Biology Commons](#), [Laboratory and Basic Science Research Commons](#), and the [Physiology Commons](#)

Recommended Citation

Al Tarhuni, Mohammed K., "Comprehensive Topological, Geometric, And Hemodynamic Analysis Of The Rat Gluteus Maximus Arteriolar Networks" (2016). *Electronic Thesis and Dissertation Repository*. 4109. <https://ir.lib.uwo.ca/etd/4109>

This Dissertation/Thesis is brought to you for free and open access by Scholarship@Western. It has been accepted for inclusion in Electronic Thesis and Dissertation Repository by an authorized administrator of Scholarship@Western. For more information, please contact wlsadmin@uwo.ca.

Abstract

The objective of this thesis was to measure the geometric and topological properties of complete arteriolar networks within skeletal muscle, and to use these data as ideal inputs in a computational blood flow model in order to analyze the corresponding hemodynamic properties. Specifically, we sought to measure the levels of structural and hemodynamic heterogeneity exhibited within and between arteriolar networks. Intravital videomicroscopy was used to image and construct photomontages of complete arteriolar networks of the rat gluteus maximus muscle under baseline conditions. Arteriolar diameters, lengths, and inter-connections were analyzed and grouped according to a centrifugal ordering scheme. For all networks considered, high levels of inter-network homology were observed with regards to the structure (geometry, topology, fractal dimension) as well as the hemodynamic (blood flow, hematocrit distribution) properties. Blood flow was proportional to the diameter cubed in support of Murray's Law. Future studies will aim to incorporate capillary and venule data in order to construct a complete model of the microcirculation within the rat gluteus maximus muscle.

Keywords

Microcirculation, Skeletal muscle, Arterioles, Arteriolar network, Intravital videomicroscopy, Blood flow, Hematocrit, Mathematical modelling, Fractal, Geometry, Topology

Co-Authorship Statement

Chapter 2 has been submitted and accepted for publication in the journal *Microcirculation*. All experiments and data collection were conducted by Mohammed Al Tarhuni. Dr. Jackson and Dr. Goldman formulated the conception and design of the experiments, assisted in the interpretation and presentation of the results, and provided overall guidance for the project. Baraa Al-Khazraji assisted with surgical training required necessary for experimental data collection.

Chapter 3 is currently in preparation for submission to the journal *Microcirculation*. The experimental data for this chapter comes primarily from chapter 2, as well as a previous publication from our laboratory in which the data were collected and analyzed by Baraa Al-Khazraji. Dr. Goldman provided the computational blood flow code, with some modifications incorporated by Mohammed Al Tarhuni. All simulations and analysis of the results were performed by Mohammed Al Tarhuni, with overall guidance and assistance in interpretation provided by Dr. Goldman and Dr. Jackson.

Acknowledgments

Throughout the course of this graduate degree, I came across many colleagues and fellow students that helped make this journey an incredible experience and a unique opportunity for academic as well as personal growth and development.

I was incredibly fortunate to have not one, but two incredibly gifted and invested supervisors, Dr. Dwayne Jackson and Dr. Daniel Goldman. Together, your endless support, encouragement, and guidance gave me the confidence and belief necessary to completing this degree. Above all, I appreciate your mentorship and thank you both for taking the time to sharing your wisdom and experiences with me at every opportunity. I have grown as much as a scholar and scientist as I have as a human being and person, and I owe much of that to training under your supervision.

Thank you to my fellow members of the Jackson and Goldman research groups for continuing to motivate and encourage me for the past two years. Graduate school comes with many hills and valleys, and your support was important to helping me navigate through this up-and-down journey. A special note of thanks goes out to Dr. Baraa Al-Khazraji for playing a pivotal role in my laboratory training, and for setting the bar for excellence in our lab.

Thank you to the wonderful administration and faculty of Medical Biophysics, and to the many people working tirelessly behind the sciences to make the lives of us graduate students just a little bit easier.

I sincerely thank my thesis examiners Dr. Chris Ellis, Dr. Kevin Shoemaker, and Dr. Susan Huang for taking the time to thoroughly review and provide essential feedback on my thesis.

Lastly, to my family and friends, thank you for always being there for me. Your mere presence in my life, in addition to your endless support and concern for my well-being, helped me get to where I am today.

Table of Contents

Abstract.....	ii
Co-Authorship Statement.....	iii
Acknowledgments.....	iv
Table of Contents.....	v
List of Tables.....	vii
List of Figures.....	viii
List of Appendices.....	ix
Chapter 1.....	1
1.1 Introduction & Background.....	1
1.2 Why have a microcirculation?.....	1
1.3 The roles of the different parts of the microcirculation.....	3
1.4 Structure of microcirculatory beds in various tissues.....	4
1.5 Quantitative descriptions of microcirculatory network geometry and topology in skeletal muscle.....	7
1.6 From structure to function – role of theoretical blood flow modeling in microvascular studies.....	12
1.7 Theoretical blood flow models.....	13
1.8 Estimating unknown boundary conditions.....	14
1.9 Towards a “network approach” for microcirculation research.....	15
1.10 Purpose of thesis dissertation.....	16
1.11 References.....	17
Chapter 2.....	25
2 Comprehensive <i>in situ</i> analysis of arteriolar network geometry and topology in rat gluteus maximus muscle.....	25

2.1 Introduction.....	26
2.2 Materials and Methods.....	27
2.3 Results.....	33
2.4 Discussion.....	45
2.5 Conclusion	48
2.6 References:.....	49
Chapter 3.....	53
3 Hemodynamic analysis of arteriolar networks in the rat gluteus maximus muscle.....	53
3.1 Introduction.....	54
3.2 Materials and Methods.....	55
3.3 Results.....	60
3.4 Discussion.....	69
3.5 Conclusion	72
3.6 References.....	73
Chapter 4.....	75
4 Contributions and Future Work	75
4.1 Contributions	75
4.2 Future Work.....	77
4.3 References.....	78
Appendix A – Figure Permissions	79
Appendix B – Animal Use Protocol Approval	82
Curriculum Vitae	83

List of Tables

Table 1: Horton's ratios for several types of tissues.	11
Table 2: Arteriolar responses to changes in O ₂ saturation (21%) and topical application of SNP (10 ⁻⁵ M).....	31
Table 3: Diameter, length, and bifurcation ratios (Horton's Laws) according to three inputs.....	37
Table 4: Distribution of ratios for all networks studied (input 2).....	37
Table 5: Summary of mean diameters and lengths at each order, with associated variability.....	40
Table 6: Segment-to-Element ratio for orders 1-9.....	44
Table 7: Characteristics of the arteriolar network models.....	61
Table 8: Relationship between blood flow and arteriolar diameter.....	63
Table 9: Comparison of structural and hemodynamic properties between mean of all networks and network 7.....	69

List of Figures

Figure 1: Visual comparison of microvascular networks in different tissues and species.	5
Figure 2: Comparison of centrifugal and centripetal ordering schemes.	10
Figure 3: Comparison of centrifugal and centripetal ordering schemes.	32
Figure 4: Gluteus maximus muscle preparation and corresponding photomontage.....	34
Figure 5: Relationships between mean internal luminal diameter (top), vessel element length (middle), and number of elements (bottom) and order.....	35
Figure 6: Comparison of mean diameter, length, and number of elements between predicted (using diameter, length, and bifurcation ratios - input 3) and observed.....	39
Figure 7: Frequency distributions of diameters for vessels of order 2-9.	42
Figure 8: Frequency distributions of lengths for vessels of order 2-9.	43
Figure 9: Fractal analysis of arteriolar networks.	45
Figure 10: Schematic of node-segment representation in a simplified arteriolar network.	56
Figure 11: Relationship between mean blood flow and topological order.	62
Figure 12: Log-log relationship between blood flow and arteriolar diameter.	63
Figure 13 (A&B): Relationship of mean blood flow between networks at orders 1-4 (A) and 5-9 (B), with average intra-network variability expressed above each group.	65
Figure 14: Relationship of mean outlet blood flow between networks.	66
Figure 15: Relationship between mean hematocrit of all networks and order.	67
Figure 16: Comparison of effective network resistance (R_{tot}) between networks.....	68

List of Appendices

Appendix A: Figure Permissions	75
Appendix B: Animal Use Protocol Approval	78

List of Abbreviations

ANOVA: Analysis of variance

CV: Coefficient of variation

D: Arteriolar diameter

D_f : Fractal dimension

GM: Gluteus maximus

H_D : Discharge hematocrit

H_T : Tube hematocrit

IVVM: Intravital video-microscopy

L: Arteriolar length

PRU: Peripheral resistance units

PSS: Physiological salt solution

Q: Blood flow rate

\mathcal{R}_{tot} : Effective network resistance

RBC: Red blood cell

R_B : Bifurcation ratio

R_D : Diameter ratio

R_L : Length ratio

SNP: Sodium nitroprusside

SNS: Sympathetic nervous system

WSS: Wall shear stress

μ_{pl} : Plasma viscosity in a vessel segment

μ_{rel} : Relative blood viscosity in a vessel segment

Chapter 1

1.1 Introduction & Background

This chapter introduces the reader to the microcirculation and its general characteristics and functions, primarily in the context of arteriolar networks within skeletal muscle. Brief notes on historical events that highlight the accomplishments of the pioneers of the field of microcirculation are presented when appropriate. Previous studies of skeletal muscle arteriolar network morphology and hemodynamics are discussed in order to present what is currently known, what limitations or improvements are possible, and the underlying motivation and merit driving the research behind this thesis.

1.2 Why have a microcirculation?

The main function of the cardiovascular system is to transport oxygenated blood from the heart to the peripheries, allowing for delivery and exchange of nutrients and hormones, and removal of metabolic waste products and deoxygenated blood from the tissues. The basic setup of the cardiovascular system is such that large conduit vessels (arteries) are ultimately connected to the smallest blood vessels, known as the capillaries, through a branching network of progressively smaller vessels on the arterial side supplying the capillaries. The capillaries are then drained by a mirroring/juxtaposing branching network of progressively larger vessels (veins) on the venous side of the circulation. Bulk transport of blood occurs through the large vessels, from the heart to the tissues through arteries and large arterioles, and from the tissue level back to the heart through large venules and veins. This type of transport is mostly convective in nature, allowing for blood to travel long distances efficiently [71].

Exchange of nutrients and metabolic waste occurs primarily at the tissue/organ level, and it is here where the microcirculation resides and plays an important role in the living animal [42]. Exchange of nutrients occurs through processes of diffusion, active cellular transport, and convection by water passing through the walls of the microvessels [57]. The microcirculation is designed to facilitate optimal exchange by virtue of the

microvessels being situated in close proximity with the parenchyma and active cells of the tissue/organ [71]. This intimate connection between the microvasculature and tissue/organ is essential to matching the blood flow to the moment-to-moment metabolic demand of the tissue/organ [57,71].

Definitions of where the macro-circulation ends (small artery) and the micro-circulation begins (large arterioles) vary [6,13,51,73] and depend on the species, type of tissue, as well as the condition under which the microvessels were studied (i.e. resting vs. maximal diameter) [42]. However, a good initial approximation is that the microcirculation begins with those blood vessels that are too small to be seen with the naked eye. Indeed, in 1628, approximately 30 years prior to the development of the first single lens microscope, the English physician William Harvey first postulated the existence of the microcirculation as a hypothesis to explain the then unknown mode of passage of blood from the arterial to the venous sides of the circulation [42]. This revolutionary hypothesis was confirmed approximately 30 years later with the pioneering work of the Italian biologist and microscopist Marcello Malpighi, who was the first to directly observe discrete capillaries in the tortoise lung with the aid of a microscope, and the Dutch scientist Antonie van Leeuwenhoek, who was the first to measure and provide quantitative descriptions on the size and dimensions of the microvessels in the tail fin of the eel [42]. Today, various quantitative cutoffs for diameters have been used to classify a blood vessel as part of the microcirculation, with an upper limit usually on the order of a few hundred micrometers (100-300 μm) in diameter considered a good estimate [71].

An interesting characteristic of the microcirculation true to all mammalian species is that the smallest microvessels (capillaries) as well as the red blood cells travelling through them are relatively very similar in size, regardless of the starting size of the feed artery or arteriole entering the tissue [95]. For example, the inferior gluteal artery, which supplies one half of the gluteus maximus muscle, is several orders of magnitude larger in diameter in the human (3-4 mm) than the mouse (65-85 μm) or the rat (120-140 μm) [6]. However, in all 3 species, the microvasculature eventually progresses down to a similar sized minimal blood vessel diameter of the capillaries (approximately 4-8 μm in diameter), and is occupied with a similar sized red blood cell (approximate diameter of 8 μm ,

volume/surface area varies slightly from human to rat to mouse) that often must deform in shape to squeeze through very small capillaries [3,42]. This is an important characteristic of the microcirculation as the majority of skeletal muscle microvascular research has been completed in small animals such as the mouse, rat, hamster, and cat [6].

1.3 The roles of the different parts of the microcirculation

Within the microcirculation, certain morphological characteristics of the microvessels allow for their classifications into three rather distinct types of vessels: arterioles, capillaries, and venules. Based on the location of these vessels within the microcirculatory bed as well as their anatomical properties, three distinct roles of these vessels came to light.

The arterioles, composed of a relatively thick layer of vascular smooth muscle and dense innervation of sympathetic nerve fibers, are the principal site of regulation and control of delivery of blood to specific tissue areas [4,73]. The decrease in diameter from the feed arteriole and progressively through the network of branching arterioles leads to a large increase in vascular resistance and a corresponding decrease in pressure. This leads to arterioles often being referred to as “resistance vessels” [65,92,99]. Terminal arterioles deliver blood to parallel networks of thin microvessels, the capillaries. Composed of a single layer of endothelium that is surrounded by a basement membrane and lacking a smooth muscle layer, the capillaries are designed for optimal exchange between blood and tissue [54,57]. Draining the capillaries are the venules, which form a network of branching vessels that mirrors that of the arterioles, although venules are generally more numerous and significantly larger in diameter at equal levels of the microcirculatory network compared to arterioles [36,79]. The venules, specifically the post-capillary venules with diameters less than $\sim 50 \mu\text{m}$, play an important role in immunological defense as well as offering some post-capillary vascular resistance and exchange of macromolecules [52,55]. Venules also play a role in venular-arteriolar communication that provides feedback of the metabolic state of the tissue for the purposes of flow regulation [30,88].

The main thrust of the network concept in microcirculatory physiology is therefore to reinforce the framework of the microvascular bed as an internally organized functional system rather than an accumulation of loosely interrelated vessel segments. Thus, it is imperative to note that characterizing all microvessels simply based on the nomenclature “arteriole”, “capillary”, or “venule” is not sufficient, as there is a high overlap in function that exists between these three types of vessels. For example, a significant level of oxygen diffusion occurs within the arterioles [32,80], the capillaries may be involved in communicating or originating vasomotor signals typically attributed to arterioles [4], and exchange of large proteins occurs predominantly in the post-capillary venules [49]. Hence, the development of more detailed classification schemes of blood vessels based on their microanatomy, geometry (diameter), and topology (location within a network) was necessary in order to better define and compare the roles of certain microvessels within the network as a whole, as well as across different types of tissues and species. These ordering schemes and how they contribute to characterizing arteriolar network structures are described in section 1.5.

1.4 Structure of microcirculatory beds in various tissues

A feature of microcirculatory networks that is consistent across all types of tissues and species is the relatively high level of heterogeneity in overall structure and design [5,15,16,63,66,71]. Simply observing any microcirculatory network immediately reveals that these complex collections of microvessels are not ideal symmetric networks forming perfectly predictable and organized structures (Figure 1). This is a natural consequence of the demand of matching the layout of the microvessels to the functional requirements of the various regions of the tissue supplied [66,71]. As a result, the overall architecture of microcirculatory networks differs based on the functional properties and state of the tissue supplied, in addition to being affected by active remodeling and adaptation to better meet the demands of the changing micro-environment [8,69].

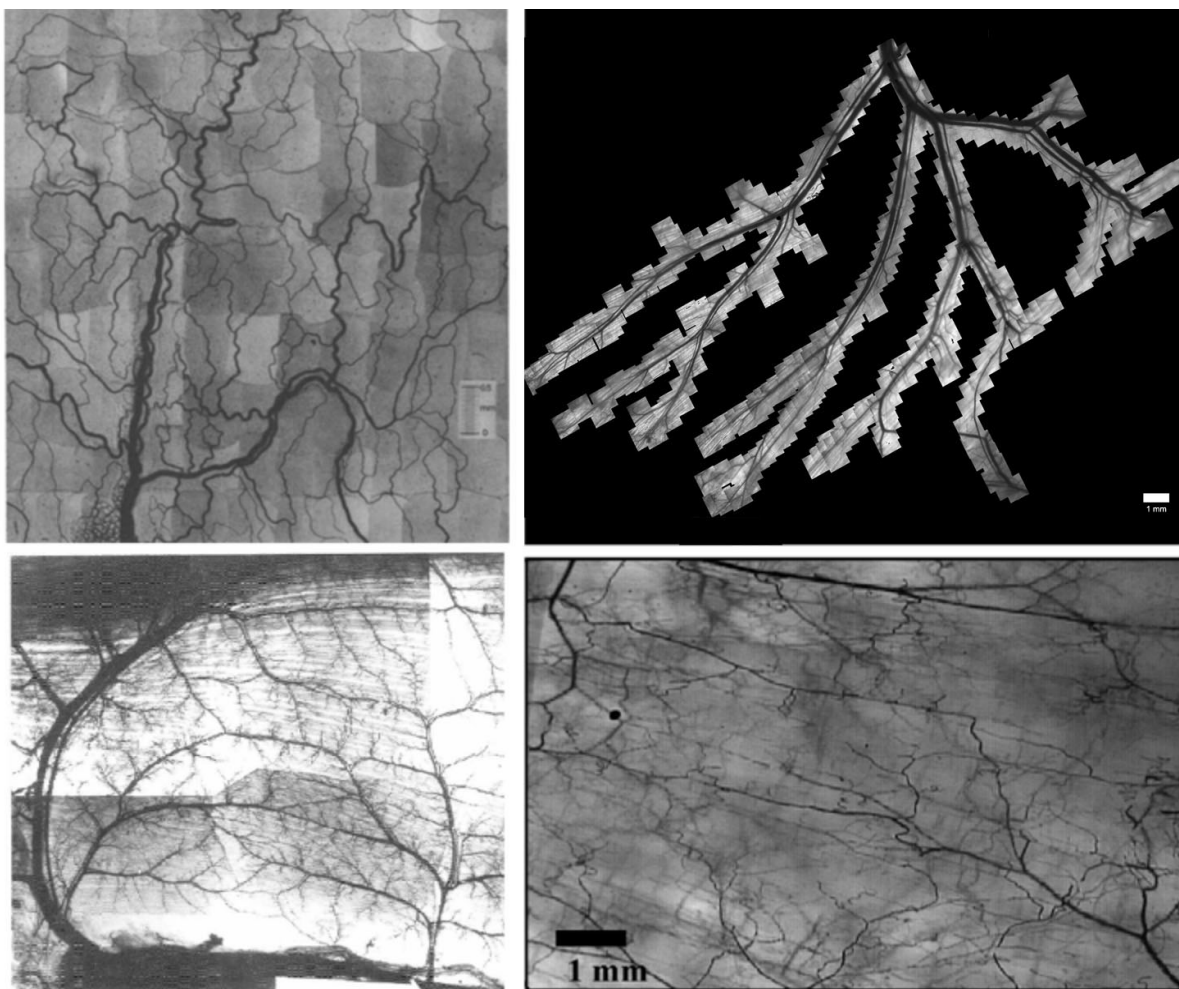


Figure 1: Visual comparison of microvascular networks in different types of tissues and species.

Top left: Rat mesentery [53]. Top right: Rat gluteus maximus [1]. Bottom left: Cat sartorius [38]. Bottom right: Pig triceps brachii [29]. The rat mesentery and gluteus maximus photomontages were obtained using IVVM, while the cat sartorius and pig triceps brachii were imaged using Microfil vascular casting techniques. Figures used with permissions (See Appendix A).

The microcirculation in the skin is organized as two horizontal plexuses, each supplying distinct regions of the skin, and connected by ascending arterioles and descending venules [11]. This type of organization is markedly different than the coronary microcirculation, where arterioles branch at close to right angles from penetrating arteries and progress in longitudinal or oblique paths towards muscle fibers [45]. The diversity of microcirculatory architecture is furthermore exhibited in the liver [94], kidney [50], brain [37], and other organs, each optimally designed to match the functional requirements of

the organ. One way that “fine-tuning” of the microcirculation to match the functional demands is exemplified is by the types of capillaries present in the microcirculatory bed. Skeletal muscle contain capillaries that are termed “continuous” due to the tight coupling of the endothelial cells allowing only small molecules to diffuse through [77]. Kidneys contain “fenestrated” capillaries, which have pores in the endothelial cells allowing trans-endothelial transport [39], while the liver contains “discontinuous” or “sinusoidal” capillaries, which have even larger pores in the endothelium and thus allow for permeability of molecules as large as erythrocytes and white blood cells to permeate the vasculature [77,93].

As a result of the varying characteristics of the three-dimensional organization and microanatomy of the microcirculatory bed from organ to organ, one must be careful to assume that observations in one type of microcirculatory bed apply to other types of tissues, or even within the same tissue but in different species. A classic example of this type of error comes from observations in one of the most popular and heavily used preparations for intravital studies of the microcirculation, the mesentery preparation [24,101], and the controversy surrounding the existence of “precapillary sphincters and metarterioles” in the microcirculation. Based on the studies of the renowned microvascular researcher Benjamin Zweifach of the mesentery in the frog, rabbit, and dog from 1937 to 1953, precapillary sphincters (valve-like folds comprised of endothelium at the point where a capillary branch leaves an arteriole) and metarterioles (thoroughfare channels connecting arterioles and venules) were indeed observed and reported [12,100,102,103], and further supported by similar observations from other researcher [74]. However, modern physiology and histology textbooks have adopted these unique elements of the mesenteric microcirculation as universal components of the microcirculation [10,41], in spite of a tremendous amount of subsequent research in a vast number of organs such as skeletal muscle [46,82], heart [31,89], lung [76], kidney [72], and several other types of tissue that have demonstrated overwhelming evidence for the lack of precapillary sphincters and metarterioles in organs other than the mesentery [74]. Curiously, modern physiology and histology textbooks, published as recently as 2009, continue to use schematics which are often reproduced from Zweifach’s original

articles depicting precapillary sphincters and metarterioles in the microcirculatory bed and identifying them as general features of the microcirculation [10].

1.5 Quantitative descriptions of microcirculatory network geometry and topology in skeletal muscle.

One of the earliest studies attempting to present detailed quantitative descriptions of microvascular network geometry and topology was conducted by the American physician Franklin Paine Mall in 1887 [10]. Although the study investigated the microcirculation of the small intestine of the dog, it nevertheless laid the foundation for future morphological studies of skeletal muscle microvasculature by providing a method for detailed measurements of diameters and number of vessels with respect to their rank (order) in the microcirculatory bed.

Comprehensive quantitative studies of the geometric and topological features of microvascular networks are fundamental towards understanding the corresponding functional properties of these networks, as the geometric and topological structure of the microvascular network and its hemodynamic properties are intimately linked [66]. Many morphological studies of skeletal muscle as well as other types of tissues have been conducted in the past. The skeletal muscle preparations that were used for these studies include the rat (gracilis [29], cremaster [9,84], spinotrapezius [19,20], soleus [98], and digitorum longus [98]), cat (tenuissius [21], sartorius [14,48]), hamster (cheek pouch retractor [17,43,87], cremaster [47]), mouse (gluteus maximus [7]), frog (sartorius [58,91]), and guinea pig (diaphragm [85]), amongst others. These studies investigated various portions of the microcirculatory bed (arteriolar, capillary, and/or venular networks) in varying degrees of quantitative detail with respect to measurements of diameter, length, branching angles, and number of segments, as well as topology (vessel inter-connections). These varying levels of detail reflect the original purpose of the study, as only a few of these studies were designed in order to collect useful geometric and topological data for incorporation as parameter inputs into mathematical models of blood flow, oxygen transport, or regulation.

The majority of current understanding of arteriolar network geometry and topology within skeletal muscle comes primarily from three studies investigating the distal (terminal) arteriolar networks. These studies were performed in the rat spinotrapezius muscle [20], the cat sartorius muscle [48], and the hamster cheek pouch retractor muscle [17]. Additionally, a follow-up report to the original study of the cat sartorius muscle terminal arteriolar networks was conducted in order to analyze the anastomosing/arcading portion of the arteriolar network of this muscle [14]. In fact, these arcading vessels are what give rise to the terminal arteriolar networks, and therefore, together form the complete arteriolar network embedded within the cat sartorius muscle. Thus, due to this additional investigation, the arteriolar networks within the cat sartorius muscle are perhaps the most completely described skeletal muscle arteriolar networks to date.

In these quantitative studies of the terminal arteriolar networks, detailed information is presented on the diameters, lengths, and number of vessels comprising the networks, as well as their inter-connections (topology). Ordering schemes are applied in order to assign certain arteriolar vessels into topological orders. The two most extensively used ordering schemes are the centrifugal (Wiedeman) and the centripetal (Horton-Strahler) ordering schemes [42,61]. These ordering schemes are derived from the mathematical field of graph theory, where in mathematical terms, the vascular bifurcation points serve as nodes or vertices, and the vessel segments in between bifurcations serving as edges. Modifications to both schemes have been made in recent studies by including certain geometric and/or topological criteria in order to better classify and group similar vessels into the same order [40,44,45,62,90].

The centrifugal ordering scheme (Figure 2) was developed in 1963 by Mary P. Wiedeman and applied in her morphological study of the subcutaneous microcirculation of the bat wing [96,97]. It has since been the most common ordering scheme used in morphological studies of the microcirculation [42]. In this scheme, order 1 is assigned to the largest arteriole feeding the tissue or the network, with progressively higher orders assigned to daughter vessels originating further downstream towards the capillaries if sufficient changes in bifurcation angle and/or diameter occurs. A modification of the centrifugal ordering scheme that is commonly applied in mesenteric networks is to

eliminate the bifurcation angle and diameter criteria, and thus increase the topological order for every daughter vessel emerging from bifurcations in the network [27,33,53]. Centrifugal ordering schemes offer the advantage of reliably comparing arterioles at different levels of the network by preserving a great amount of topological and geometric information. However, the diameter and/or angle criteria for designating a branch as a new order is inherently subjective, and must be carefully considered when data are compared from different laboratories.

The centripetal (Horton-Strahler) scheme (Figure 2) was adapted from the geomorphological literature pertaining to the analysis of river networks by Robert E. Horton in 1945 [35] and subsequently modified by Arthur Newell Strahler in 1952 [86]. Bruce Fenton and Benjamin Zweifach first applied this modified version to studies of microvascular morphology in 1981 in their investigations of the rabbit omentum and human bulbar conjunctiva [23]. This scheme begins by assigning order 1 to the terminal pre-capillary arterioles, and progressively higher orders are assigned to larger caliber arterioles when daughter vessels of the same order converge upstream towards the feed arteriole and form a parent vessel. This ordering scheme is ideal for terminal arteriolar networks, as they are conveniently located next to capillary beds. It is also ideal for asymmetric networks with side branches that are much smaller in diameter in comparison to neighboring main branches, as these side branches will often be appropriately classified into lower orders than the neighboring but much larger main branches. However, this ordering scheme is purely topological (i.e. classifies vessels purely on location within the network) and requires the identification of all terminal arteriolar vessels prior to beginning, making it less practical for classifications of large arteriolar networks [42].

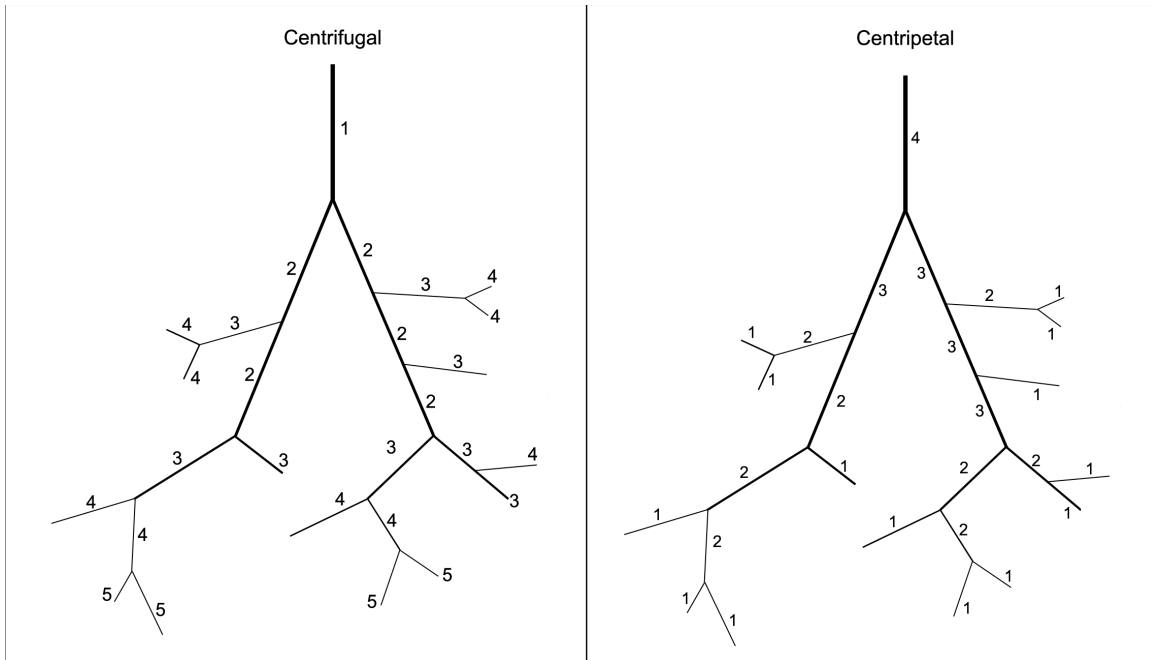


Figure 2: Comparison of centrifugal and centripetal ordering schemes.

Application of these ordering schemes results in relationships known as Horton's Laws, originally derived from the morphological studies of river networks. These laws state that the diameters, lengths, and number of vessels follow power-law relationships with respect to the topological order, i.e. a linear relationship is observed when the logarithm of the diameter, length, or number of vessels is plotted as a function of topological order. In all three studies of the cat sartorius muscle, hamster cheek pouch muscle, and the rat spinotrapezius muscle, Horton's laws were shown to be valid with the application of the Horton-Strahler ordering scheme in the terminal arteriolar networks [18,20,48]. The resulting ratios derived from Horton's Laws (R_B - Bifurcation Ratio, R_L - Length Ratio, R_D - Diameter Ratio) are presented in Table 1 as well as ratios from non-skeletal muscle and non-vascular tissue.

Table 1: Horton's ratios for several types of tissues.

Tissue	R_B	R_L	R_D	Reference
Skeletal Muscle				
Cat sartorius	3.17	1.86	1.25	[48]
Rat spinotrapezius	2.74	1.33	1.51	[20]
Hamster cheek pouch retractor	3.43	2.59	1.63	[17]
Non-Skeletal Muscle				
Human pulmonary arteries	2.99	1.49	1.59	[83]
Human bulbar conjunctiva	2.77	1.36	1.26	[23]
Rabbit omentum	3.12	1.61	1.3	[23]
Non-vascular tissue				
Rat bronchial tree	3.31	1.82	1.53	[34]
Human bronchial tree	2.81	1.4	1.43	[34]

The major limitations from these fundamental studies of skeletal muscle arteriolar network structure stem from the approach used to collect the geometric and topological data, as well as the inherent anatomy of the skeletal muscle preparations used. In the cases of the hamster cheek pouch retractor and the rat spinotrapezius arteriolar networks, the microcirculation was perfused with corrosion casting material that requires maximal vasodilation of the vessels. Thus, the diameters reported in these studies are at their maximal values and do not reflect the native state of the microcirculation. Secondly, in all three studies, the networks that were studied were the terminal/distal arteriolar networks. These terminal networks are a collection of a relatively small number of arteriole segments, with an extremely narrow range of diameters from terminal ($\sim 5 \mu\text{m}$) to feed ($\sim 20\text{-}30 \mu\text{m}$) arterioles. The terminal arteriolar networks originate from transverse arterioles that branch from a network of larger arcading/looping arterioles, which are

themselves supplied by several feed arteries that provide the bulk blood supply to the muscle tissue [6,20]. It has been shown that these arcading networks of larger arterioles function as a protective mechanism to maintain adequate blood supply to the tissue in the case that one or more of the feeding arterioles are occluded [18]. However, their presence in these skeletal muscle preparations presents a limitation to this type of analysis, as they must be analyzed separately from the terminal arteriolar networks due to the presence of closed loops and arcades.

The rat gluteus maximus (GM) skeletal muscle preparation is an ideal preparation for overcoming these limitations. The thinness and planar geometry of the muscle allows for its microcirculation to be readily observed without the infusion of any fixatives or vasodilatory substances (i.e. under baseline native conditions) in high resolution with bright-field trans-illumination [1,7]. In addition, the GM is supplied by only two feed arteries (inferior and superior gluteal arteries) that form two independent tree-like networks. These networks each act to supply approximately one-half of the muscle, and rarely contain closed loops or arcades [6].

1.6 From structure to function – role of theoretical blood flow modeling in microvascular studies

A common approach to quantitatively analyze the hemodynamic properties (blood flow, red blood cell distribution, oxygen transport, etc.) of large microcirculatory networks is to combine experimental data with theoretical approaches. In blood flow modeling, a typical approach is to use experimentally derived data on the structural properties (diameters, lengths, vessel connectivity) of microcirculatory networks in conjunction with known biophysical laws of flow (Poiseuille's law [59,60,67]) as well as empirically derived relationships of the particulate nature of blood in microvessels (Fahreus effect, Phase-separation effect, Fahreus-Linqvist effect [64,67,68]) in order to predict the distribution of blood flow and hematocrit within a network. Predictions of blood flow and hematocrit are necessary due to the fact that measurements of certain parameters such as red blood cell velocity, intravascular pressure, or wall shear stress in networks with hundreds or even thousands of individual segments is difficult or impractical; thus we must rely on

theoretical models to obtain complete self-consistent estimates of network hemodynamics [25,70].

Theoretical modeling of blood flow has added a wealth of novel information to the study of the microcirculation because of its ability to predict and infer the functional responses of microcirculatory networks in a variety of conditions that may be difficult to replicate or measure experimentally [81]. For example, our laboratory has extended the experimental findings regarding the level of dependence of sympathetic nervous system mediated vasoconstriction on topological order to compute the resulting functional impact on blood flow and hematocrit distribution under both healthy conditions in the skeletal muscle of the rat [2], as well as pre-diabetic conditions in the mouse (Novielli, N. et al, 2016, in preparation). Experimental studies of microvascular control and regulation provide novel understanding on the mechanisms controlling blood flow, but they are enhanced with the use of theoretical modeling as this combination allows for understanding of the global functional response of the microvascular network to the measured perturbations.

1.7 Theoretical blood flow models

With the development of any theoretical model, a primary goal is to validate the predictions of the simulations with comparisons to experimentally measured data [81]. A model is then validated if its predictions are found to be consistent with experimental measurements. Many theoretical models have been developed for simulating blood flow in both individual microvessels as well as microvascular networks [22,23,26,38,56,78,80]. One of the most popular blood flow models for the study of microvascular network hemodynamics was developed by Axel Pries and his colleagues from the observations of blood flow in the rat mesentery [67,68].

This theoretical model was built by using intravital video microscopy to obtain the geometric and topological structure of the microcirculation of the rat mesentery, as well as microphotometric techniques for the measurement of tube and discharge hematocrit values. The model also incorporated parametric descriptions relating to the particulate

nature of blood in microvessels (Fahreus effect, Phase-separation effect, Fahraeus-Linqvist effect) based upon empirically derived measurements [68]. Model results are computed using an iterative procedure that alternatively solves for hemodynamic parameters (blood flow, pressure) followed by rheological parameters (hematocrit, viscosity) until convergence to steady-state values is found in all vessel segments of the network. This iterative procedure is necessary due to the non-linear dependence of viscosity on local hematocrit and of red blood cell distribution at bifurcations on blood flow distribution.

Boundary conditions, in the form of pressure or flow values at the inlet and outlet vessels, are necessary for solving the model equations. In the realistic case where not all boundary conditions are known, as is usually the case with large networks [25], a method is necessary in order to estimate the boundary conditions.

1.8 Estimating unknown boundary conditions

In this thesis, we used a novel approach for estimating unknown boundary conditions in large arteriolar networks with missing boundary conditions that was based upon three recent studies.

The first study was from our laboratory, where a novel *in vivo* method was used to measure the RBC velocity profiles in branching arteriolar trees (diameters 21-115 μm) of the rat gluteus maximus [1]. The data from this study were used to fix the total (inlet) flow for each simulation.

The least squares optimization approach of Fry et al. was then used to minimize the deviation of pressure and wall shear-stress values in the network given target values for the pressure at all nodes and the wall shear stresses in all sub-segments [25]. A limitation of this approach occurs when target shear stresses and pressure values must be guessed due to lack of experimental data.

Therefore, a further improvement to the Fry method was developed in our laboratory to address this limitation [28,75]. In this approach, the Fry method is modified by

performing a second set of iterations in order to find the target wall shear stress values needed to match the total blood flow that was measured experimentally. The target pressure value is set to one-half the mean pressure in the network after each iteration.

1.9 Towards a “network approach” for microcirculation research

The inherent geometric, topological, and hemodynamic heterogeneity exhibited within virtually all microvascular networks is the main driving force behind adopting a “network” approach to microcirculatory research. This is due to the fact that data acquired from local/point-source perturbations, combined with the use of mean or typical values for geometric or hemodynamic parameters to estimate unknown values, can lead to incorrect conclusions regarding overall tissue structure and/or function [70]. Thus, the idea behind a network approach would be, in the ideal scenario, to collect all, or at least a sufficiently large sample, of the relevant geometric, topological, and hemodynamic parameters of the network in order to reliably interpret and predict the effect of local perturbations to overall network function and tissue perfusion.

While the network approach is ideal in theory, it is extremely challenging, and thus it perhaps should not be surprising that it has not been adopted widely as evidenced by the dearth of complete microvascular network structure and hemodynamic databases for many of the microcirculatory beds previously studied. Some of the challenges to this approach include requiring skeletal muscle preparations that readily allow access to complete microvascular networks, imaging techniques and processing tools that allow for the visualization of the complete network and its inter-connections in high resolution, as well as experimental measurements of all the pertinent structural and hemodynamic parameters in networks with 100s to even 1000s of individual segments.

The incredibly comprehensive and collaborative research of Axel Pries, Timothy Secomb, Peter Gaehtgens, and their many collaborators on the structure and function of microcirculation of the rat mesentery has made it currently the most completely described network from a structural as well as hemodynamic perspective. A similar approach

leading to a comprehensive database is desperately lacking for microcirculatory networks of skeletal muscle, as making inferences from the mesentery to skeletal muscle is not ideal. Development of such a database and model would greatly advance the understanding of skeletal muscle vascular physiology in both healthy and pathological conditions.

1.10 Purpose of thesis dissertation

The motivation behind this project is to generate a “mean” model of skeletal muscle arteriolar networks for the purposes of better understanding the blood flow behavior in the microcirculation of skeletal muscle.

The first step in accomplishing this goal was to describe the geometric and topological structure of the complete arteriolar network of the rat gluteus maximus muscle. Data on the diameters, lengths, and connectivity of the vessel segments of the network were measured under baseline *in situ* conditions, and used to analyze the variability within and between networks.

Using the experimentally measured data on the structure of the arteriolar networks of the rat gluteus maximus, as well as previously measured *in vivo* data related to blood flow velocities, we determined the functional behavior of the arteriolar networks using computational blood flow modeling. Based on the structural and hemodynamic characteristics obtained for a number of networks, we selected a representative arteriolar network that best encompasses all the relevant parameters that were measured or estimated, and may serve as a “mean” model network for future studies of skeletal muscle arteriolar network structure, hemodynamics, and regulation.

1.11 References

1. Al-Khazraji BK, Novielli NM, Goldman D, Medeiros PJ, Jackson DN. A simple “streak length method” for quantifying and characterizing red blood cell velocity profiles and blood flow in rat skeletal muscle arterioles. *Microcirculation* **19**: 327-335, 2012.
2. Al-Khazraji BK, Saleem A, Goldman D, Jackson DN. From one generation to the next: a comprehensive account of sympathetic receptor control in branching arteriolar trees. *The Journal of physiology* **593**: 3093-3108, 2015.
3. Altman P, Dittmer D. Blood and Other Body Fluids Federation of American Societies for Experimental Biology. *Washington, DC*: 186, 1961.
4. Bagher P, Segal SS. Regulation of blood flow in the microcirculation: role of conducted vasodilation. *Acta physiologica* **202**: 271-284, 2011.
5. Bassingthwaighte JB. Physiological heterogeneity: fractals link determinism and randomness in structures and functions. *Physiology* **3**: 5-10, 1988.
6. Bearden SE. Effect of aging on the structure and function of skeletal muscle microvascular networks. *Microcirculation* **13**: 279-288, 2006.
7. Bearden SE, Payne GW, Chisty A, Segal SS. Arteriolar network architecture and vasomotor function with ageing in mouse gluteus maximus muscle. *The Journal of physiology* **561**: 535-545, 2004.
8. Benoit JN, Granger DN. Intestinal microvascular adaptation to chronic portal hypertension in the rat. *Gastroenterology* **94**: 471-476, 1988.
9. Bohlen HG, Gore RW, Hutchins PM. Comparison of microvascular pressures in normal and spontaneously hypertensive rats. *Microvascular research* **13**: 125-130, 1977.
10. Boron WF, Boulpaep EL. Medical physiology: a cellular and molecular approach. Philadelphia, PA: Saunders. In, edn: Elsevier, 2009.
11. Braverman IM. The cutaneous microcirculation: ultrastructure and microanatomical organization. *Microcirculation* **4**: 329-340, 1997.
12. Chambers R, Zweifach B. Topography and function of the mesenteric capillary circulation. *American Journal of Anatomy* **75**: 173-205, 1944.
13. Charny C. Advances in Heat Transfer Bioengineering Heat Transfer. 1992.

14. Cyrino F, Popel A, Bouskela E, Johnson P. Morphometric analysis of the anastomosing arteriolar network in cat sartorius muscle. *International Journal of Microcirculation* **14**: 3-13, 1994.
15. Duling BR. Is red cell flow heterogeneity a critical variable in the regulation and limitation of oxygen transport to tissue? In: *Oxygen Transport to Tissue XVI*: Springer, 1994, p. 237-247.
16. Duling BR, Damon DH. An examination of the measurement of flow heterogeneity in striated muscle. *Circulation research* **60**: 1-13, 1987.
17. Ellsworth M, Liu A, Dawant B, Popel A, Pittman R. Analysis of vascular pattern and dimensions in arteriolar networks of the retractor muscle in young hamsters. *Microvascular research* **34**: 168-183, 1987.
18. Ellsworth ML, Liu A, Dawant B, Popel AS, Pittman RN. Analysis of vascular pattern and dimensions in arteriolar networks of the retractor muscle in young hamsters. *Microvasc Res* **34**: 168-183, 1987.
19. Engelson E, Schmid-Schönbein G, Zweifach B. The microvasculature in skeletal muscle. III. Venous network anatomy in normotensive and spontaneously hypertensive rats. *International journal of microcirculation, clinical and experimental/sponsored by the European Society for Microcirculation* **4**: 229-248, 1984.
20. Engelson ET, Skalak TC, Schmid-Schönbein GW. The microvasculature in skeletal muscle: I. Arteriolar network in rat spinotrapezius muscle. *Microvascular research* **30**: 29-44, 1985.
21. Eriksson E, Myrhage R. Microvascular dimensions and blood flow in skeletal muscle. *Acta Physiologica Scandinavica* **86**: 211-222, 1972.
22. Fenton BM, Wilson DW, Cokelet GR. Analysis of the effects of measured white blood cell entrance times on hemodynamics in a computer model of a microvascular bed. *Pflügers Archiv* **403**: 396-401, 1985.
23. Fenton BM, Zweifach B. Microcirculatory model relating geometrical variation to changes in pressure and flow rate. *Annals of Biomedical Engineering* **9**: 303-321, 1981.
24. Frasher WG, Wayland H. A repeating modular organization of the microcirculation of cat mesentery. *Microvascular research* **4**: 62-76, 1972.
25. Fry BC, Lee J, Smith NP, Secomb TW. Estimation of blood flow rates in large microvascular networks. *Microcirculation* **19**: 530-538, 2012.
26. Furman M, Olbricht W. Unsteady cell distributions in capillary networks. *Biotechnology progress* **1**: 26-32, 1985.

27. Gaehtgens P, Ley K, Pries A. Topological approach to the analysis of microvessel structure and hematocrit distribution. 1986.
28. Goldman D, Saleem AH, Al-Khazraji BK, Jackson DN. Estimating Blood Flow in Skeletal Muscle Arteriolar Trees Reconstructed from In Vivo Data. *The FASEB Journal* **30**: 947.942-947.942, 2016.
29. Gruionu G, Hoying JB, Gruionu LG, Laughlin MH, Secomb TW. Structural adaptation increases predicted perfusion capacity after vessel obstruction in arteriolar arcade network of pig skeletal muscle. *American journal of physiology Heart and circulatory physiology* **288**: H2778-2784, 2005.
29. Henrich HN, Hecke A. A gracilis muscle preparation for quantitative microcirculatory studies in the rat. *Microvascular research* **15**: 349-356, 1978.
30. Hester RL, Hammer LW. Venular-arteriolar communication in the regulation of blood flow. *American Journal of Physiology-Regulatory, Integrative and Comparative Physiology* **282**: R1280-R1285, 2002.
31. Higuchi K, Hashizume H, Aizawa Y, Ushiki T. Scanning electron microscopic studies of the vascular smooth muscle cells and pericytes in the rat heart. *Archives of histology and cytology* **63**: 115-126, 2000.
32. Honig CR, Gayeski T, Clark A, Clark P. Arteriovenous oxygen diffusion shunt is negligible in resting and working gracilis muscles. *Am J Physiol-Heart C* **261**: H2031-H2043, 1991.
33. Horsfield K. Diameters, generations, and orders of branches in the bronchial tree. *J Appl Physiol* **68**: 457-461, 1990.
34. Horsfield K, Thurlbeck A. Volume of the conducting airways calculated from morphometric parameters. *Bulletin of mathematical biology* **43**: 101-109, 1981.
35. Horton RE. Erosional development of streams and their drainage basins; hydrophysical approach to quantitative morphology. *Geol Soc Am Bull* **56**: 275-370, 1945.
36. House SD, Johnson PC. Diameter and blood flow of skeletal muscle venules during local flow regulation. *Am J Physiol-Heart C* **250**: H828-H837, 1986.
37. Hudetz AG. Blood flow in the cerebral capillary network: a review emphasizing observations with intravital microscopy. *Microcirculation* **4**: 233-252, 1997.
38. Hudetz AG, Spaulding JG, Kiani MF. Computer simulation of cerebral microhemodynamics. In: *Oxygen Transport to Tissue XI*: Springer, 1989, p. 293-304.

39. Ichimura K, Stan RV, Kurihara H, Sakai T. Glomerular endothelial cells form diaphragms during development and pathologic conditions. *Journal of the American Society of Nephrology* **19**: 1463-1471, 2008.
40. Jiang Z, Kassab G, Fung Y. Diameter-defined Strahler system and connectivity matrix of the pulmonary arterial tree. *J Appl Physiol* **76**: 882-892, 1994.
41. Johnson LR. *Essential medical physiology* edn: Academic Press, 2003.
42. Johnson PC. Overview of the microcirculation. In, edn: Amsterdam, Elsevier, 2008, p. 6-20.
43. Joyner WL, Davis MJ, Gilmore JP. Intravascular pressure distribution and dimensional analysis of microvessels in hamsters with renovascular hypertension. *Microvascular research* **22**: 190-198, 1981.
44. Kassab GS, Berkley J, Fung Y-CB. Analysis of pig's coronary arterial blood flow with detailed anatomical data. *Annals of biomedical engineering* **25**: 204-217, 1997.
45. Kassab GS, Rider CA, Tang NJ, Fung Y-C. Morphometry of pig coronary arterial trees. *Am J Physiol-Heart C* **265**: H350-H365, 1993.
46. Klitzman B, Damon D, Gorczynski R, Duling B. Augmented tissue oxygen supply during striated muscle contraction in the hamster. Relative contributions of capillary recruitment, functional dilation, and reduced tissue PO₂. *Circulation Research* **51**: 711-721, 1982.
47. Klitzman B, Johnson PC. Capillary network geometry and red cell distribution in hamster cremaster muscle. *Am J Physiol-Heart C* **242**: H211-H219, 1982.
48. Koller A, Dawant B, Liu A, Popel A, Johnson P. Quantitative analysis of arteriolar network architecture in cat sartorius muscle. *The American journal of physiology* **253**: H154-164, 1987.
49. Korthuis RJ. *Microvascular Fluid and Solute Exchange in Skeletal Muscle*. 2011.
50. Kriz W, Kaissling B. Structural organization of the mammalian kidney. *The kidney: physiology and pathophysiology* **1**: 265-306, 1992.
51. Kuo L, Davis MJ, Chilian WM. Myogenic activity in isolated subepicardial and subendocardial coronary arterioles. *Am J Physiol-Heart C* **255**: H1558-H1562, 1988.
52. Ley K. Adhesion molecules and the recruitment of leukocytes in postcapillary venules. *Microvascular Research: Biology and Pathology*: 321-325, 2005.

53. Ley K, Pries A, Gaehtgens P. Topological structure of rat mesenteric microvessel networks. *Microvascular research* **32**: 315-332, 1986.
54. Majno G. Ultrastructure of the vascular membrane. *Handbook of physiology* **3**: 2293-2375, 1965.
55. Ohashi K, Tung DL, Wilson J, Zweifach B, Schmid-Schönbein G. Transvascular and interstitial migration of neutrophils in rat mesentery. *Microcirculation* **3**: 199-210, 1996.
56. Papenfuss H, Gross J. Microhemodynamics of capillary networks. *Biorheology* **18**: 673-692, 1980.
57. Pittman RN. Influence of microvascular architecture on oxygen exchange in skeletal muscle. *Microcirculation* **2**: 1-18, 1995.
58. Plyley M, Sutherland GJ, Groom A. Geometry of the capillary network in skeletal muscle. *Microvascular research* **11**: 161-173, 1976.
59. Poiseuille JLM. Recherches sur la force du coeur aortique. 1828.
60. Poiseuille JLM. *Recherches sur les causes du mouvement du sang dans les veines* edn: impr. H. Tilliard, 1830.
61. Popel A. Network models of peripheral circulation. *Handbook of Bioengineering*: 20.21-20.24, 1987.
62. Popel A, Torres FI, Johnson P, Bouskela E. A new scheme for hierarchical classification of anastomosing vessels. *International journal of microcirculation, clinical and experimental/sponsored by the European Society for Microcirculation* **7**: 131-138, 1988.
63. Popel AS, Johnson PC. Microcirculation and hemorheology. *Annual review of fluid mechanics* **37**: 43, 2005.
64. Pries A, Ley K, Claassen M, Gaehtgens P. Red cell distribution at microvascular bifurcations. *Microvascular research* **38**: 81-101, 1989.
65. Pries A, Secomb T. Control of blood vessel structure: insights from theoretical models. *Am J Physiol-Heart C* **288**: H1010-H1015, 2005.
66. Pries A, Secomb T, Gaehtgens P. Structure and hemodynamics of microvascular networks: heterogeneity and correlations. *Am J Physiol-Heart C* **269**: H1713-H1722, 1995.
67. Pries A, Secomb T, Gaehtgens P, Gross J. Blood flow in microvascular networks. Experiments and simulation. *Circulation research* **67**: 826-834, 1990.

68. Pries A, Secomb T, Gessner T, Sperandio M, Gross J, Gaehtgens P. Resistance to blood flow in microvessels in vivo. *Circulation research* **75**: 904-915, 1994.
69. Pries AR, Cornelissen AJ, Sloot AA, Hinkeldey M, Dreher MR, Höpfner M, Dewhirst MW, Secomb TW. Structural adaptation and heterogeneity of normal and tumor microvascular networks. *PLoS Comput Biol* **5**: e1000394, 2009.
70. Pries AR, Secomb TW. Microcirculatory network structures and models. *Annals of biomedical engineering* **28**: 916-921, 2000.
71. Pries AR, Secomb TW. Blood flow in microvascular networks. *Comprehensive Physiology*, 2011.
72. Sakai F, Kriz W. The structural relationship between mesangial cells and basement membrane of the renal glomerulus. *Anatomy and embryology* **176**: 373-386, 1987.
73. Sakai H, Hara H, Tsai AG, Tsuchida E, Intaglietta M. Constriction of resistance arteries determines L-NAME-induced hypertension in a conscious hamster model. *Microvascular research* **60**: 21-27, 2000.
74. Sakai T, Hosoyamada Y. Are the precapillary sphincters and metarterioles universal components of the microcirculation? An historical review. *The Journal of Physiological Sciences* **63**: 319-331, 2013.
75. Saleem AH. Estimating Hemodynamics in Skeletal Muscle Arteriolar Networks Reconstructed From In Vivo Data. M.Sc. Thesis. University of Western Ontario, London, 2015.
76. Sasaki S-I, Kobayashi N, Dambara T, Kira S, Sakai T. Structural organization of pulmonary arteries in the rat lung. *Anatomy and embryology* **191**: 477-489, 1995.
77. Scallan J, Huxley VH, Korthuis RJ. Capillary Fluid Exchange: Regulation, Functions, and Pathology. *Colloquium Series on Integrated Systems Physiology: From Molecule to Function* **2**: 1-94, 2010.
78. Schmid-Schönbein G, Skalak R, Usami S, Chien S. Cell distribution in capillary networks. *Microvascular research* **19**: 18-44, 1980.
79. Schmid-Schönbein G, Skalak T, Engelson E, Zweifach B. Microvascular Network Anatomy in Rat Skeletal Muscle¹. 1986.
80. Secomb T, Hsu R. Simulation of O₂ transport in skeletal muscle: diffusive exchange between arterioles and capillaries. *Am J Physiol-Heart C* **267**: H1214-H1221, 1994.

81. Secomb TW, Beard DA, Frisbee JC, Smith NP, Pries AR. The role of theoretical modeling in microcirculation research. *Microcirculation* **15**: 693-698, 2008.
82. Segal SS. Regulation of blood flow in the microcirculation. *Microcirculation* **12**: 33-45, 2005.
83. Singhal S, Henderson R, Horsfield K, Harding K, Cumming G. Morphometry of the human pulmonary arterial tree. *Circulation Research* **33**: 190-197, 1973.
84. Smaje L, Zweifach B, Intaglietta M. Micropressures and capillary filtration coefficients in single vessels of the cremaster muscle of the rat. *Microvascular research* **2**: 96-110, 1970.
85. Spector WS. Handbook of biological data. *Handbook of biological data*, 1956.
86. Strahler AN. Quantitative analysis of watershed geomorphology. *Eos, Transactions American Geophysical Union* **38**: 913-920, 1957.
87. Sullivan SM, Pittman RN. Hamster retractor muscle: a new preparation for intravital microscopy. *Microvascular research* **23**: 329-335, 1982.
88. Tigno XT, Ley K, Pries AR, Gaehtgens P. Venulo-arteriolar communication and propagated response. *Pflügers Archiv* **414**: 450-456, 1989.
89. Tsunenari I. [Cushion-like structure in coronary arteries of rats]. *Kaibogaku zasshi Journal of anatomy* **68**: 67-75, 1993.
90. Turcotte D, Pelletier J, Newman W. Networks with side branching in biology. *Journal of theoretical biology* **193**: 577-592, 1998.
91. Tymi K, Ellis CG, Safranyos RG, Fraser S, Groom AC. Temporal and spatial distributions of red cell velocity in capillaries of resting skeletal muscle, including estimates of red cell transit times. *Microvascular research* **22**: 14-31, 1981.
92. VanTeeffelen JW, Segal SS. Interaction between sympathetic nerve activation and muscle fibre contraction in resistance vessels of hamster retractor muscle. *The Journal of physiology* **550**: 563-574, 2003.
93. Vollmar B, Menger MD. The hepatic microcirculation: mechanistic contributions and therapeutic targets in liver injury and repair. *Physiological reviews* **89**: 1269-1339, 2009.
94. Wanless IR. Physioanatomic considerations. *Schiff's Diseases of the Liver, Eleventh Edition*: 87-119, 2003.
95. West GB, Brown JH, Enquist BJ. A general model for the origin of allometric scaling laws in biology. *Science* **276**: 122-126, 1997.

96. Wiedeman MP. Dimensions of blood vessels from distributing artery to collecting vein. *Circulation research* **12**: 375-378, 1963.
97. Wiedeman MP. Blood flow through terminal arterial vessels after denervation of the bat wing. *Circulation research* **22**: 83-90, 1968.
98. Williams DA, Segal SS. Microvascular architecture in rat soleus and extensor digitorum longus muscles. *Microvascular research* **43**: 192-204, 1992.
99. Yuan SY, Rigor RR. Structure and function of exchange microvessels. 2010.
100. Zweifach B, Shorr E, Black M. The influence of the adrenal cortex on behavior of terminal vascular bed. *Ann Ny Acad Sci* **56**: 626-633, 1953.
101. Zweifach BW. The structure and reactions of the small blood vessels in Amphibia. *American Journal of Anatomy* **60**: 473-514, 1937.
102. Zweifach BW. The character and distribution of the blood capillaries. *The Anatomical Record* **73**: 475-495, 1939.
103. Zweifach BW. Basic mechanisms in peripheral vascular homeostasis. *Factors regulating blood pressure Transactions of the third conference May*. pp 5-6, 1949.

Chapter 2

Comprehensive *in situ* analysis of arteriolar network geometry and topology in rat gluteus maximus muscle

A form of this manuscript has been published in the journal *Microcirculation*:

Al Tarhuni M, Goldman D, Jackson DN. Comprehensive *in situ* analysis of arteriolar network geometry and topology in rat gluteus maximus muscle. *Microcirculation*. 2016.

2.1 Introduction

In skeletal muscle microcirculation, arterioles play two distinct roles in hemodynamic regulation, which are dependent on diameter and/or topological arrangement. Altering resistance in larger bore (proximal) arterioles tends to modify total bulk blood flow to the tissue; while altering resistance in smaller bore (distal) arterioles plays a pivotal role in modifying red blood cell (RBC) distribution to downstream capillary networks [36].

Due to the inverse power law relationship between arteriolar diameter and resistance, studies measuring only arteriolar radius at bifurcations have dominated skeletal muscle blood flow research. Microvascular studies using IVVM (*in situ*) or isolated vessels (*in vitro*) have commonly investigated arteriolar regulation/dysregulation using local ‘point-source’ interrogation at arteriolar bifurcations [12,17,32]. Although data from such studies have shaped our understanding of microvascular control, the contribution of local arteriolar responses to global changes in total network resistance, blood flow, and RBC distribution is commonly left to inference or speculation.

For decades, theoretical modelers have stressed that quantitative analysis of the distribution of microvascular blood flow and hematocrit requires a detailed description of the vascular network geometry [10]. In fact, hemodynamic characteristics of microvascular networks can only be adequately described if both topological and geometric variability in network structure are taken into account [35]. Although several studies have endeavored to characterize the geometry and topology of skeletal muscle arteriolar networks, their analyses have been limited to small microvascular segments with narrow ranges of arteriolar diameters. For example, geometric analysis of terminal arteriolar branching in the cat sartorius [22] as well as the hamster cheek pouch muscle [10] has been reported, however such studies have been limited to examining only the most distal arterioles, with diameters ranging from $\sim 10\text{-}30\ \mu\text{m}$. Some earlier studies have analyzed larger/complete microvascular networks. However, they employed vascular casting, a process requiring pharmacological vasodilation of the arterioles (prior to casting) [8,11,38], which limits the interpretation, application, and scope of their findings.

We have established the rat gluteus maximus (GM) preparation as a novel experimental model to directly study integrative skeletal muscle hemodynamics in branching microvascular networks using intravital video microscopy (IVVM) [1]. The planar geometry and uniform thickness of the GM enable access (within a single focal plane) to its entire microcirculation for imaging and perturbation. Additionally, the rat GM is a skeletal muscle that is recruited during locomotion, common to all mammalian species and to both sexes, and is made of a mixed fibre type composition [3,8]. These properties of the rat GM make it an ideal skeletal muscle preparation for intravital studies of skeletal muscle vascular physiology and hemodynamics.

Based on the current dearth of geometrically accurate and complete microvascular network data, the goal of the present study was to provide a quantitative account of the rat gluteus maximus arteriolar network *in situ* under baseline conditions, and to assess the level of geometric/topological heterogeneity across networks from different animals. Parameters such as diameter and length as well as overall structure and branching pattern are assessed, as they are an essential requirement for computational studies of skeletal muscle hemodynamics [34].

2.2 Materials and Methods

Animal Care and use:

The Council on Animal Care at Western University approved all animal procedures. Experiments were performed on 8 male Sprague-Dawley rats (aged 8-9 weeks; mean \pm SD mass: 303 \pm 15 g), purchased from Charles River Laboratories (Saint-Constant, Quebec, Canada) and housed on site for at least 1 week prior to the study. Rats were housed in Western University's animal care facilities under a 12:12 h light/dark cycle in temperature controlled (24°C) rooms with access to food and water *ad libitum*. Each rat was weighed at the start of each experiment. At the end of each experiment, the anaesthetized rat was sacrificed with an overdose of α -chloralose and urethane cocktail mix (i.p. injection).

Anesthesia and skeletal muscle preparation:

The rat gluteus maximus muscle preparation has been described in detail elsewhere[1]. Briefly, a cocktail of α -chloralose (80 mg/kg) and urethane (500 mg/kg) was used to anaesthetize the rat (i.p. injection), which was supplemented as needed throughout the duration of the experiment. The fur of the neck and the lower back region was shaved, and the rat was placed on a custom built temperature-controlled platform in order to maintain body temperature at 37°C (rectal probe). Surgical procedures were performed with the aid of a stereomicroscope. A mid-neck incision was made to allow insertion of a tracheal cannula (PE-50) in order to facilitate spontaneous respiration. The rat was then positioned prone and the skin covering the lower left region of the back was removed. The left gluteus maximus muscle was identified and, while taking great care taken to preserve its neurovascular supply, the muscle was delicately cut from its origin along the spine and along its rostral and caudal borders. Next, the muscle was gently reflected away from the rat onto a transparent (Sylgard 184; Dow Corning, Midland, MI, USA) pedestal, spread flat and evenly to approximate *in situ* dimensions, and the edges of the tissue were secured onto the pedestal using stainless steel fly pins. The exposed muscle was superfused continuously (4-5 ml/min) with bicarbonate-buffered physiological salt solution (PSS, 35 °C at tissue, pH 7.4) of composition (mM): 137 NaCl, 4.7 KCL, 1.2 MgSO₄, 2 CaCl₂, and 18 NaHCO₃, and equilibrated with 5% CO₂ /95% N₂ gas.

Intravital video microscopy:

Following completion of microsurgical procedures, the rat preparation was transferred to the stage of the intravital microscope (Olympus BX51; Olympus, Tokyo, Japan). To allow the preparation to stabilize, ~30 min of equilibration with PSS occurred prior to data collection, during which time the arteriolar network was mapped for sites of data collection (vasomotion was not observed). The arteriolar network was imaged under Kohler illumination using a long working distance condenser (NA=0.80) and a long working distance water immersion objective (Olympus LUMPLFL: 10x NA = 0.30; depth of field ~9 μ m) with illumination from a 100W halogen light source. A 450/20-nm band-pass filter (450BP20; Omega Optical Battleboro, VT, USA) was placed in the light path in order to enhance the contrast of the RBC column. The optical image was coupled to an EMCCD camera (Rolera EMC²; Qimaging; Surrey, BC, Canada), viewed using

specialized imaging software (MetaMorph, version 7.6; Molecular Devices Inc., Sunnyvale, CA, USA) and stored on a hard drive for future offline analysis. Following ~30 min of equilibration, the baseline internal vessel lumen diameter at several arteriolar orders was recorded and arterioles were tested for oxygen sensitivity (vasoconstriction) by elevating PSS superfusion O₂ from 0% to 21% (with 5% CO₂, balance N₂) for ~5 min and recording the arteriolar diameter (Table 2). For the duration of the experiment, the PSS superfusion was restored to 5% CO₂-95% N₂. At the end of each experiment, sodium nitroprusside (SNP, 10 μM) was added to the superfusate and maximum arteriolar diameter was recorded at several arteriolar orders. Only preparations that demonstrated robust responses to elevated oxygen and SNP levels were included in this study. The inlet feed arteriole (inferior gluteal artery) was identified and located, and bright-field video (.tiff) images were collected (17 fps) under Kohler bright-field illumination of the emerging daughter arterioles. A total microvascular area of approximately 4 cm² was imaged for each experiment.

Network montage, geometric measurements, and calculation of fractal dimensions:

Matlab (MathWorks Inc., Natick, MA, USA) was used to register individual IVVM frames together to create a photomontage of the complete arteriolar network. Approximately 500 overlapping frames were used to construct each photomontage.

ImageJ (NIH, Bethesda, MD, USA)[37] was then used to measure the arteriolar network's geometric properties (vessel diameter, lengths). A diameter measurement was made approximately every 150 μm along the length of each unbranched arteriolar segment, resulting in approximately 1500 sub-segments per network. Mean diameter for each arteriolar element (defined as the group of segments connected serially of the same topological order [23]) was calculated as the arithmetic average of the diameter measures of all sub-segments constituting that element. Element length was calculated as the sum of the length of all sub-segments constituting an element. Using MATLAB, a centrifugal ordering algorithm (with order increasing at bifurcations when a daughter vessel had a diameter <80% of parent, or a bifurcation angle >15°)[2] was applied to the network,

resulting in arterioles ranging from 1st (proximal) to 9th (distal) order in 7 of the 8 networks studied. The remaining network resulted in centrifugal orders of 1 to 8.

Using this definition of segments and elements, we measured the pattern of interconnections of the individual arterioles forming a network by calculating the average segment-to-element (S/E) ratio at each order (Figure 3). This ratio provides a measure of the level of asymmetry associated with the arterioles of a given topological order [23]. A ratio of 1 indicates an equal number of segments to elements (symmetric), while ratios greater than 1 indicate higher numbers of segments than elements (asymmetric), resulting in multiple segments of an element joining in series, with vessels belonging to the subsequent topological order originating as side branches from these serially-connected segments.

Photomontages of networks were digitized using Matlab and a skeletonized binary line tracing of the arteriolar networks was produced. *FracLac* [18], an open-source software developed for ImageJ, was used to compute the fractal dimension (D_f) using the box-counting method [25]. The box-counting method determines the number of boxes containing a vessel segment using varying box sizes, then calculates D_f from the slope of the regression line of the logarithm of the number of boxes containing a segment as a function of the logarithm of the box size. This method has been applied to vascular beds of many organs in the past to calculate the D_f [5,13,15,28,31,41].

Table 2: Arteriolar responses to changes in O₂ saturation (21%) and topical application of SNP (10⁻⁵ M)

Order	Baseline Diameter (μm)	O₂ response (μm)	SNP response (μm)
1	128 ± 3	-16 ± 3	+27 ± 5
2	92 ± 2	-10 ± 1	+26 ± 3
3	68 ± 4	-8 ± 1	+22 ± 2
4	41 ± 2	-7 ± 1	+20 ± 2
5	28 ± 1	-6 ± 1	+20 ± 2
6	20 ± 1	-6 ± 2	+19 ± 1
7	16 ± 1	-5 ± 2	+15 ± 1
8	14 ± 1	-8 ± 3	+13 ± 1
9	12 ± 1	-6 ± 3	+10 ± 1

Data presented as mean ± SEM (n=8 animals).

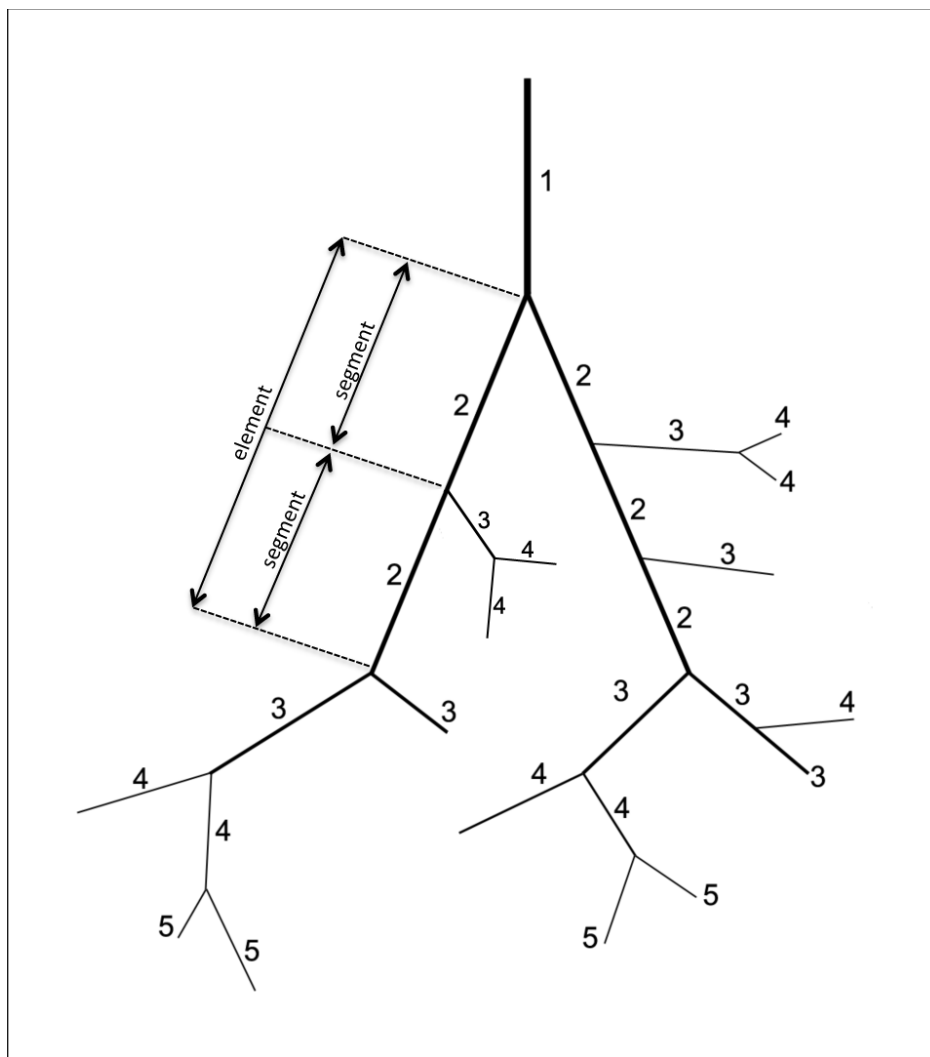


Figure 3: Comparison of centrifugal and centripetal ordering schemes.

Our centrifugal ordering algorithm assigns the main feed arteriole an order of 1 and progressively assigns higher orders when daughter vessels have diameters $< 80\%$ of the parent and/or bifurcation angles $> 15^\circ$. An arteriolar ‘segment’ is a length of arteriole situated between two successive bifurcations. An arteriolar ‘element’ is a group of serially connected arteriolar ‘segments’ within the same topological order.

Statistical Analyses:

Experimental data are presented as mean \pm SEM, unless otherwise stated. Data were analyzed using Prism software (version 6.0g, GraphPad Software Inc., La Jolla, CA, USA) and differences were accepted as significantly different at $p < 0.05$. One-way ANOVA was used to test for differences between mean diameter, length, and number of

elements between topological orders. Linear regression was performed to evaluate the correlation between the natural logarithm of diameter, length, or number of elements and the topological order. The coefficient of variability (standard deviation divided by the mean) was used to characterize the variation of mean diameter and length with respect to topological order. The inter-network variability of the mean diameter [$CV(D_{\text{mean},i})$] or length [$CV(L_{\text{mean},i})$], was calculated by determining the mean diameter ($D_{\text{mean},i}$) or length ($L_{\text{mean},i}$) of a given order for each network i ($i = 1$ to 8), followed by calculating the corresponding coefficient of variability. Similarly, the mean intra-network variability, [$\text{mean } CV_i(D_{\text{mean},i})$] or [$\text{mean } CV_i(L_{\text{mean},i})$], was calculated by first determining the coefficient of variability for the mean diameter ($D_{\text{mean},i}$) or length ($L_{\text{mean},i}$) of a given order for each network i ($i = 1$ to 8), $CV_i(D_{\text{mean},i})$ or $CV_i(L_{\text{mean},i})$, followed by averaging these CV_i values over the population of networks ($n = 8$ networks) for each topological order.

2.3 Results

Figure 4A provides a visual representation of a typical arteriolar network arising from the inferior gluteal feed artery and its location within the gluteus maximus muscle preparation. The network photomontage is constructed offline using an in-house image registration algorithm from individual IVVM frames (Figure 4B). The overall topological layout of the arteriolar network of the rat GM resembles a branching tree structure, with arcading arteriolar loops occurring rarely [7]. This overall tree-like pattern of the microvascular network is exhibited in other skeletal muscle preparations such as the cremaster [7].

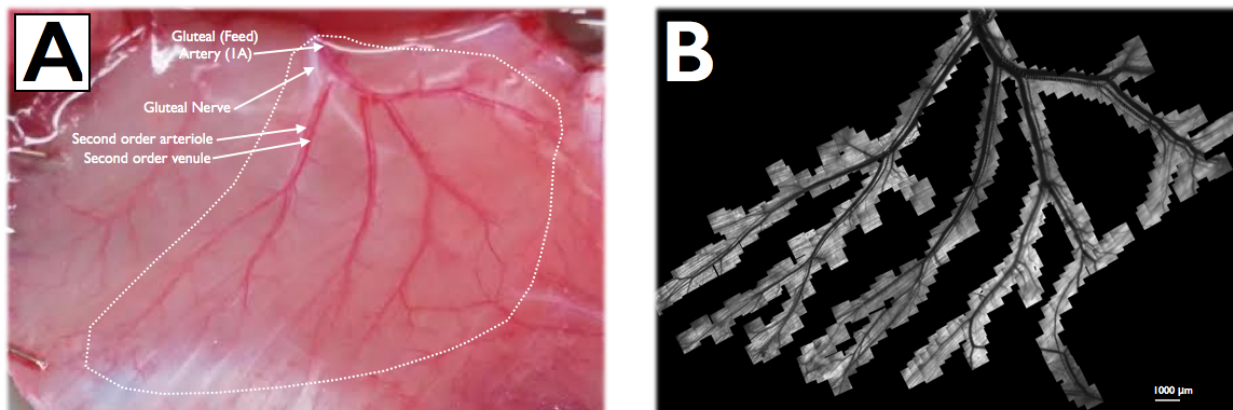


Figure 4: Gluteus maximus muscle preparation and corresponding photomontage

Location of arteriolar network studied within the rat gluteus maximus muscle (A).

Photomontage of IVVM frames (10x: 573 frames, 1004x1002 dpi) used to reconstruct complete arteriolar network (B).

The means of the internal luminal diameters (Figure 5A) and element lengths (Figure 5B) decreased with increasing vessel order. The number of elements at each vascular order increased with increasing vascular order (Figure 5C). Note that for calculation of mean lengths, 1A arterioles were excluded due to the inability to reliably measure the total length of the feed arteriole entering the skeletal muscle preparation. In figure 3C, elements of order 6,7, and 8 that were not a terminal branch were grouped into one group (non-terminal), while the remaining elements of order 6,7,8, and 9 that were true terminal branches (i.e., directly supplied capillary beds) were grouped into another group (terminal).

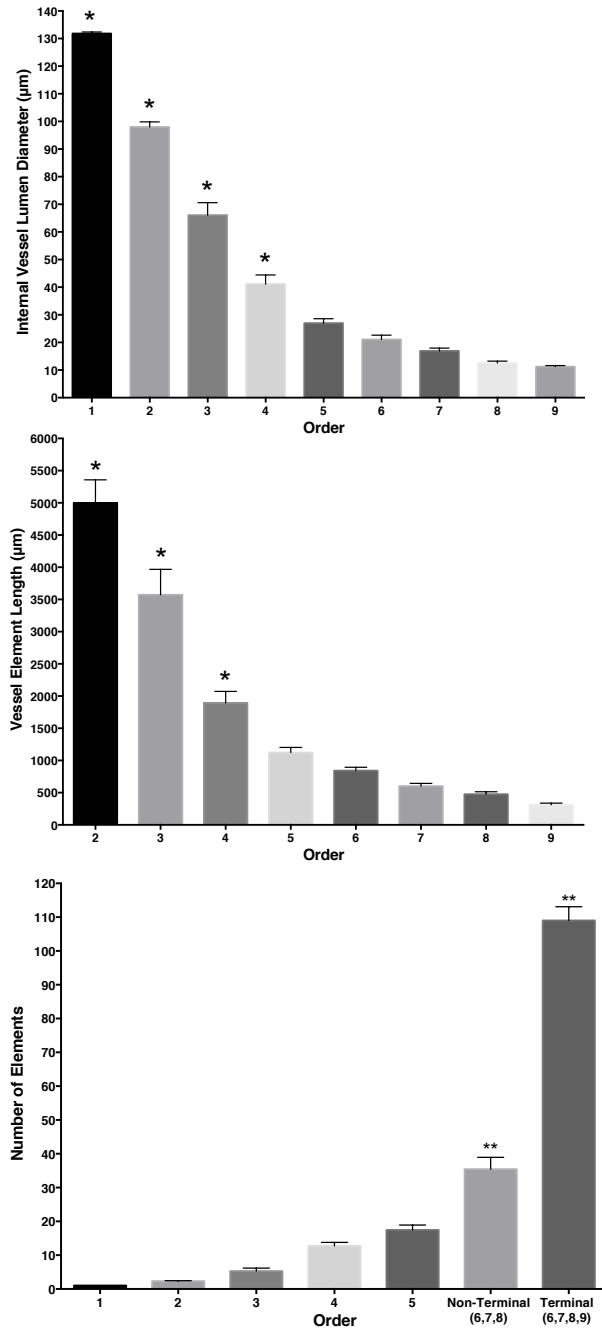


Figure 5: Relationships between mean internal luminal diameter (top), vessel element length (middle), and number of elements (bottom) and order.

Mean diameter and length decreased with increasing topological order, while number of elements increased with increasing topological order. Data presented as mean \pm SEM ($n=8$ animals). (* significantly different from subsequent order at $p < 0.05$, ** significantly different from previous order at $p < 0.05$).

To test the validity of Horton's laws in the arteriolar network of the rat GM, we performed linear regression analysis between the natural logarithm of each geometric variable (internal luminal diameter, element length, and number of elements) and topological order. Three slightly different methods (inputs) were used to calculate the diameter, length, and bifurcation ratios similar to previous studies [10,11,22].

The first input was derived using data from all networks, which were combined to calculate mean values (Table 3). Using this input, the mean internal vessel diameter (D_i) vs. the order (i) is fitted by $\ln(D_i) = 5.082 - 0.3209i$ ($i = 1$ to 9), $R^2 = 0.9748$ ($P < 0.0001$). The diameter ratio (R_{D1}) is determined by the slope of the regression line; $R_{D1} = e^{0.3209} = 1.3784$. The mean vessel element length (L_i) vs order (i) is fitted by $\ln(L_i) = 9.136 - 0.3842i$ ($i = 1$ to 9), $R^2 = 0.9763$ ($P < 0.0001$). The length ratio (R_{L1}) is determined by the slope of the regression line; $R_{L1} = e^{0.3842} = 1.4684$, $R^2 = 0.9748$ ($P < 0.0001$). The mean number of vessel elements (B_i) vs order (i) is fitted by $\ln(B_i) = 0.7045i - 0.6561$ ($i = 1$ to 7), $R^2 = 0.9878$ ($P < 0.0001$). The bifurcation ratio (R_{B1}) is determined by the slope of the regression line; $R_{B1} = e^{0.7405} = 2.0969$.

The second input was derived by performing linear regressions on the mean values (diameter, length, number of elements) vs. order for each individual network separately, followed by averaging the ratios obtained for each network over the population of networks (Table 4). The diameter ratio (R_{D2}), length ratio (R_{L2}), and bifurcation ratio (R_{B2}) according to this second definition were 1.3892, 1.4861, and 2.0980 respectively (Table 3).

Lastly, the third input was derived by averaging the mean values (diameter, length, number of elements) at each order for each individual network, followed by a linear regression analysis of the final averaged values. The diameter ratio (R_{D3}), length ratio (R_{L3}), and bifurcation ratio (R_{B3}) according to this third definition were 1.3821, 1.4860, and 2.1347 respectively (Table 3).

Table 3: Diameter, length, and bifurcation ratios (Horton's Laws) according to three inputs.

Input	Diameter (R_D)	Length (R_L)	Bifurcation (R_B)
1) Regression for all networks combined	1.3784	1.4684	2.0969
Correlation Coefficient (R^2)	0.9763	0.9748	0.9878
2) Averages of regressions of each network	1.3892	1.4861	2.1347
Correlation Coefficient (R^2)	0.9633	0.9501	0.9747
3) Regression for mean values of each network	1.3821	1.4860	2.0980
Correlation Coefficient (R^2)	0.9496	0.9182	0.9647

Table 4: Distribution of ratios for all networks studied (input 2)

Network	R_D (R^2)	R_L (R^2)	R_B (R^2)
1	1.4247 (0.98)	1.4529 (0.99)	2.1673 (0.99)
2	1.3526 (0.99)	1.4601 (0.96)	2.1385 (0.99)
3	1.3503 (0.97)	1.4102 (0.91)	1.9263 (0.95)
4	1.3788 (0.98)	1.5238 (0.96)	2.1730 (0.99)
5	1.4310 (0.95)	1.4957 (0.92)	2.3755 (0.99)
6	1.3486 (0.92)	1.4909 (0.90)	1.9423 (0.92)
7	1.3903 (0.96)	1.5135 (0.98)	2.1187 (0.96)
8	1.4372 (0.96)	1.5414 (0.98)	2.2360 (0.99)
Mean	1.3892 (0.96)	1.4861 (0.95)	2.1347 (0.97)

With all three inputs, the relationships between the natural logarithm of mean diameters, lengths, and number of elements as a function of order was strong ($R^2 \geq 0.9$), thus indicating that Horton's laws are obeyed within the arteriolar networks of the rat gluteus maximus. The ratios obtained from this analysis accurately predict the sequence of mean values of the corresponding variable (diameter, length, number of elements) from given 1st order values (Figure 6).

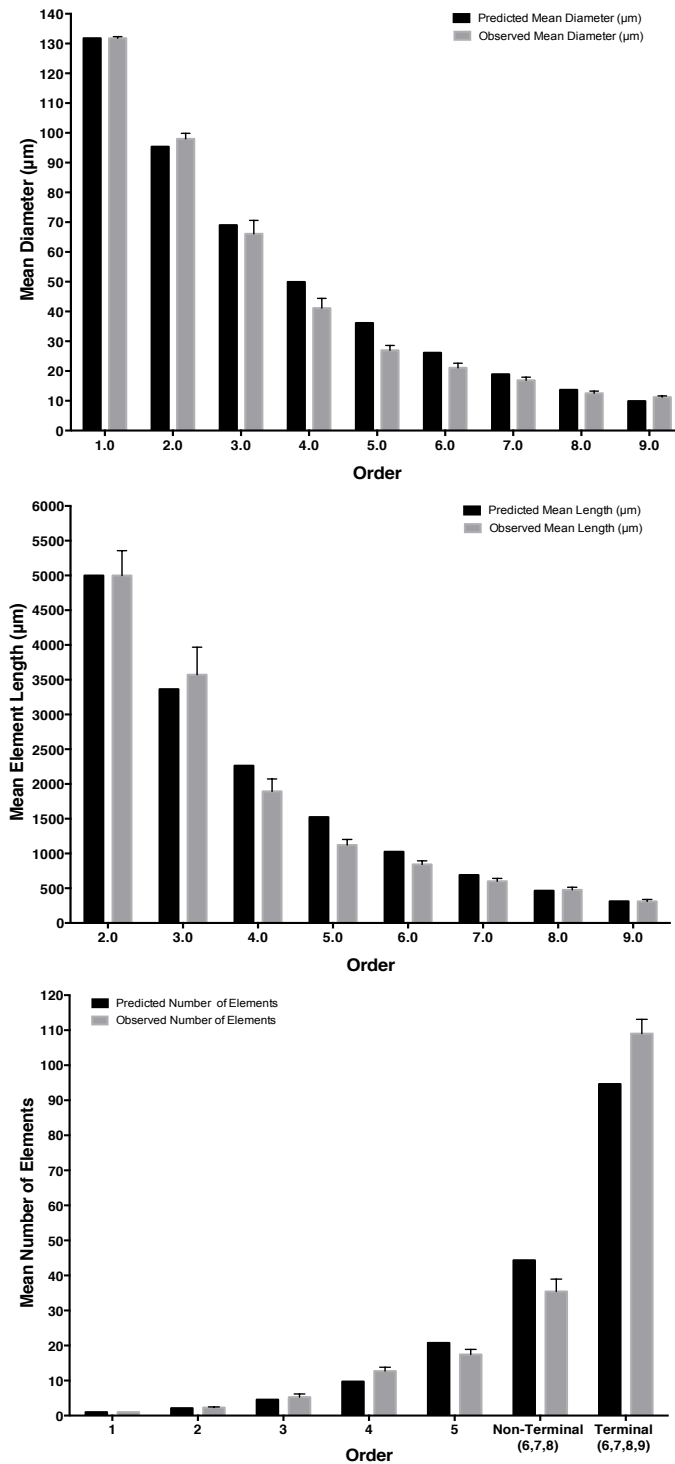


Figure 6: Comparison of mean diameter, length, and number of elements between predicted (using diameter, length, and bifurcation ratios - input 3) and observed. Data presented as mean \pm SEM (n=8 animals).

In assessing the level of variation of geometric variables (diameters, lengths) between and within networks, we found relatively lower levels of heterogeneity of mean diameters and lengths between networks (diameters: 1.17 to 22.73 %, lengths: 17.53 to 31.32%) than within networks (diameters: 9.58 to 48.54%, lengths: 38.97 to 106.01%) (Table 5). The levels of both inter-network as well as intra-network heterogeneity typically increased with increasing topological order, peaking at orders 5 and 6, followed by a decreasing trend from orders 7 to 9 (Table 5).

Table 5: Summary of mean diameters and lengths at each order, with associated variability.

Order	Mean Diameter	CV($D_{\text{mean},i}$)	Mean $CV_i(D_{\text{mean},i})$	Mean Length	CV($L_{\text{mean},i}$)	Mean $CV_i(L_{\text{mean},i})$
1	131.8	1.17%	0.00%	-	-	-
2	97.99	5.37%	9.58%	4998	20.31%	40.90%
3	66.08	19.38%	33.34%	3572	31.32%	59.35%
4	41.11	22.72%	43.35%	1893	26.80%	90.80%
5	26.96	17.16%	46.91%	1122	20.41%	100.48%
6	21.07	21.06%	48.54%	842.5	17.53%	106.01%
7	16.9	17.51%	40.56%	599.1	20.22%	80.03%
8	12.53	16.05%	30.20%	476.3	22.90%	89.07%
9	11.23	9.55%	27.77%	310	24.07%	38.97%

CV($D_{\text{mean},i}$) & CV($L_{\text{mean},i}$) represent the inter-network variability of mean diameter and length respectively. Mean $CV_i(D)$ & Mean $CV_i(L)$ represent the average intra-network variability of diameter and length respectively. Mean Diameter and Mean Length are given in μm (n=8 animals).

Frequency distributions of diameters (Figure 7) and lengths (Figure 8) at orders 2-9 were analyzed in order to further examine the dispersion of diameters and lengths at each topological order. Vessel diameters and lengths were fitted by a Gaussian distribution ($p < 0.05$) at orders 2 to 9 with high chi-square goodness-of-fit values for both diameters (2nd order: $R^2 = 0.9060$, 3rd order: $R^2 = 0.5333$, 4th to 9th order: $R^2 > 0.80$) and lengths (2nd order: $R^2 = 0.2815$, 3rd order: $R^2 = 0.3771$, 4th to 9th order: $R^2 > 0.80$).

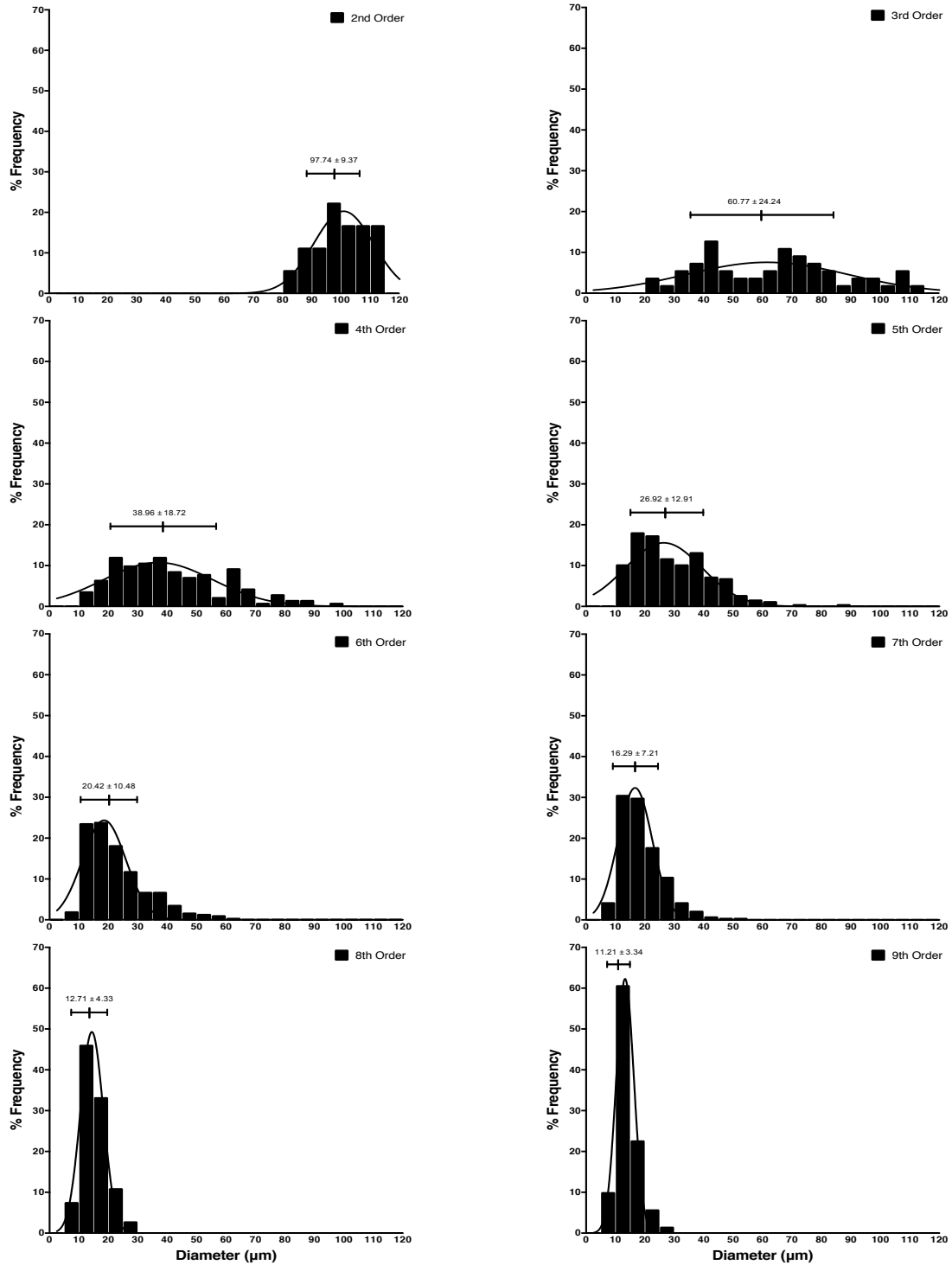


Figure 7: Frequency distributions of diameters for vessels of order 2-9.

Distributions were fit with a Gaussian function with high chi-square goodness-of-fit values (2nd order: $R^2 = 0.9060$, 3rd order: $R^2 = 0.5333$, 4th to 9th order: $R^2 > 0.80$). Center vertical line represents mean, while horizontal line represents standard deviation.

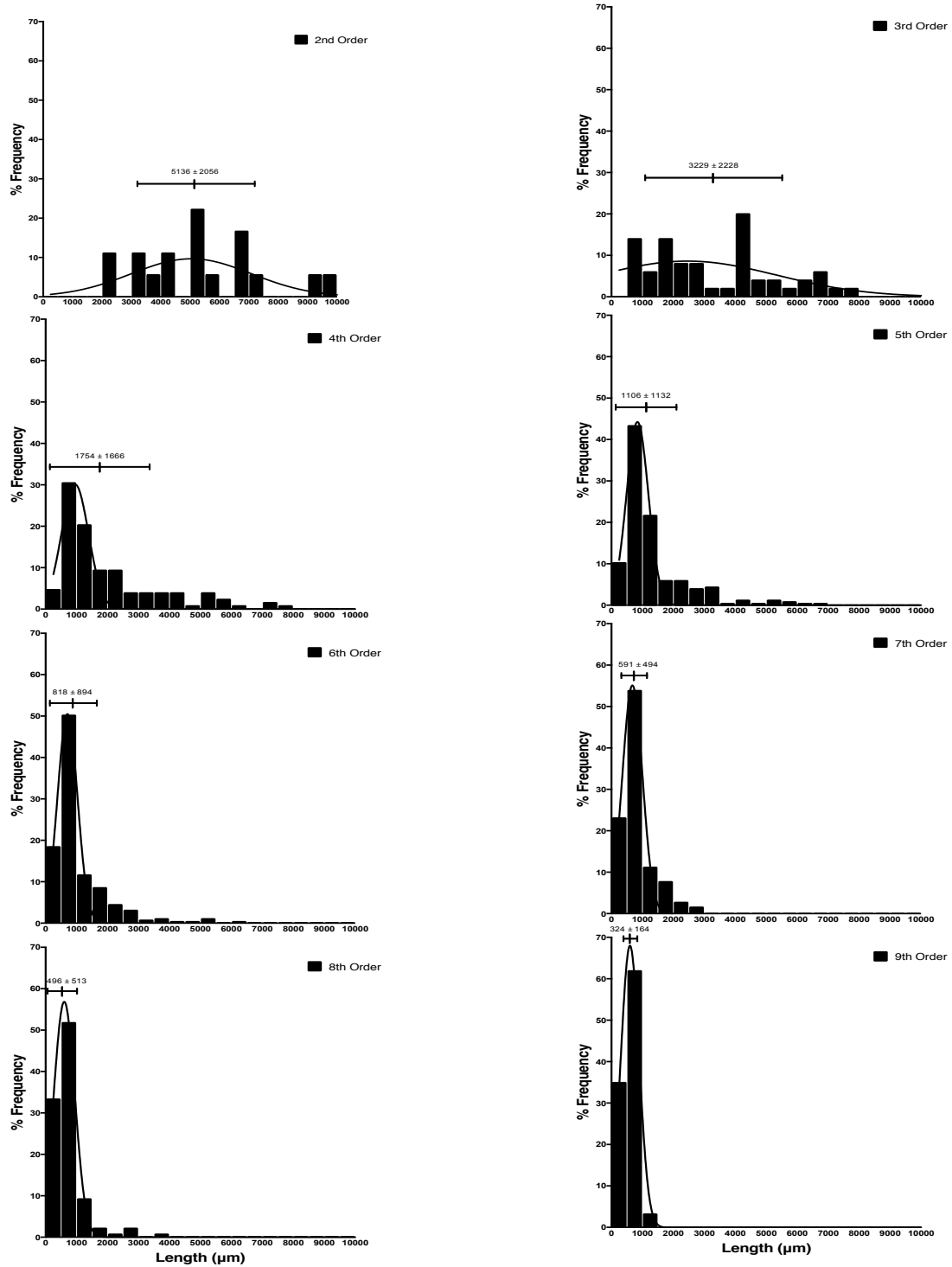


Figure 8: Frequency distributions of lengths for vessels of order 2-9.

Distributions were fit with a Gaussian function with high chi-square goodness-of-fit values (2nd order: $R^2 = 0.2815$, 3rd order: $R^2 = 0.3771$, 4th to 9th order: $R^2 > 0.80$). Center vertical line represents mean, while horizontal line represents standard deviation.

The S/E ratio was greatest in proximal (lower-order) arterioles (orders 2 to 4) and decreased towards distal (higher-order) arterioles (orders 5 to 9). The highest S/E ratio, and thus greatest asymmetry of bifurcations with regards to change in order, was found in 3rd order arterioles (Table 6).

Table 6: Segment-to-Element ratio for orders 1-9.

Order	S/E
1	1.25 ± 0.25
2	1.54 ± 0.39
3	1.94 ± 0.25
4	1.81 ± 0.28
5	1.29 ± 0.07
6	1.37 ± 0.05
7	1.18 ± 0.04
8	1.08 ± 0.02
9	1 ± 0.00

Data presented as mean ± SEM (n=8 animals).

Finally, fractal analysis was used as another tool to measure the inter-network structural homology. Fractal analysis quantitatively describes the network's spatial complexity by computing its fractal dimension – a measure of a network's vascular complexity. The arteriolar networks of the rat GM exhibited strong homology with respect to their fractal dimension (D_f : 1.3315 to 1.4202, CV of 1.86%), (Figure 9).

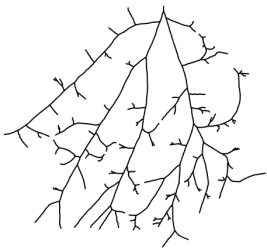
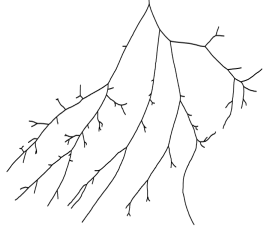
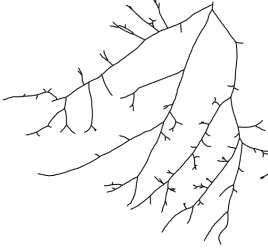
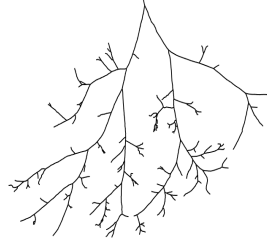
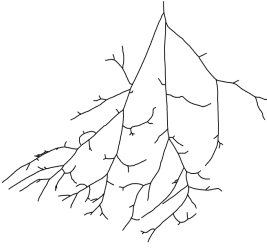
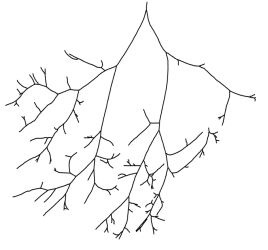
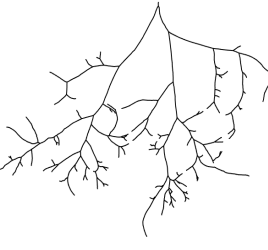
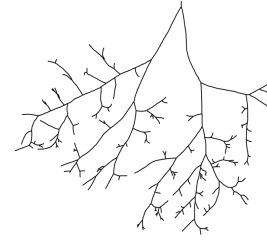
Network 1	Network 2	Network 3	Network 4
			
1.4020 ± 0.01 R ² = 0.99	1.3315 ± 0.01 R ² = 0.99	1.3851 ± 0.01 R ² = 0.99	1.3814 ± 0.01 R ² = 0.99
Network 5	Network 6	Network 7	Network 8
			
1.3907 ± 0.01 R ² = 0.99	1.3922 ± 0.01 R ² = 0.99	1.3726 ± 0.01 R ² = 0.99	1.4202 ± 0.01 R ² = 0.99

Figure 9: Fractal analysis of arteriolar networks.

Single line tracings of arteriolar networks with associated Fractal Dimensions ($D_f \pm \text{SEM}$) below each tracing. The mean \pm SEM of the D_f was 1.3844 ± 0.01 (CV = 1.86%).

2.4 Discussion

This study provides the first comprehensive and detailed analysis of the overall geometric and topological structure of arteriolar networks within the rat gluteus maximus muscle. Importantly, it is one of a few morphological studies employing IVVM to image and

record geometric data under baseline conditions, as opposed to the more traditional vascular casting technique that requires a vasodilator substance to be infused prior to data collection and analysis.

It has been shown in many vascular networks that vessel lengths, diameters, and number of elements follow a geometric sequence with respect to topological order [19,20,39]. These relationships are known as Horton's Laws [16,33]. Applying Horton's Laws to microvascular networks results in ratios that describe the change in the geometric variables (diameter, length, number of elements) between orders. Owing to the unique structure of the arteriolar network within the rat gluteus maximus, we were able to perform analysis and confirm Horton's laws over a wider range of diameters, lengths, and topological orders than previously done in other skeletal muscle preparations. We report a similar diameter (R_D : 1.38) and length ratio (R_L : 1.46) to those measured from other skeletal muscle arteriolar networks (R_D : 1.25-1.63, R_L : 1.33 to 2.59). The bifurcation ratio from our study (2.09) is smaller than previously reported from other studies (2.56 to 3.43)[10,11,22].

With regards to the levels of geometric homology between and within networks, we found relatively lower heterogeneity of mean diameters and lengths between networks (17 to 31%) than within networks (38 to 106%). The intra-network heterogeneity was highest at the middle branches of the network (orders 5 and 6). Additionally, the S/E ratio was highest (i.e. most asymmetric) in the vessels of order 3 and 4. Varying levels of geometric and topological heterogeneity of microvascular networks have been shown to lead to corresponding heterogeneity of various hemodynamic parameters such as blood flow, resistance, and RBC distribution [35]. In order to elucidate the functional consequences of the observed geometry and topology of the rat GM, and the extent to which the hemodynamics characteristics of networks vary within and between networks, a detailed study of the network hemodynamics is required.

Arteriolar networks often exhibit self-similarity by virtue of their geometric properties (diameter, lengths, elements) following a power-law relationship with respect to order [33]. It is this property of self-similarity that allows for these arteriolar networks to be

analyzed using fractal geometry principles. Indeed, fractal analysis has been performed on many microvascular networks in a variety of tissues, under both healthy and pathological conditions [5,9,24,30].

Fractal analysis has been used to characterize hemodynamic properties such as mass transport and flow distribution in many vascular networks. For example, the fractal dimension has described differences in blood flow heterogeneity in the coronary circulation among pigs [40], baboons, sheep, and rabbits [6]. As well, the fractal dimension has been used to describe the magnitude of angiogenesis and vascular remodeling in many tissues. In the chick chorioallantoic membrane, several research groups have used fractal analysis to quantify changes in microvascular structure and neovascularization due to application of angiogenesis promoting and inhibiting drugs. To illustrate, Knoll et al. reported that the fractal dimension decreased with delivery of the anti-angiogenic drug Amiloride [21] and Mancardi et al. reported that the fractal dimension increased with delivery of pro-angiogenic fibroblast growth factor (FGF) [29]. Finally, the fractal dimension has been explored in clinical applications as a quantitative measure for delineating between healthy and pathological microvascular network structure, such as in the capillary structure of the oral mucosa in patients with atrophic-erosive oral lichen planus [27], retinal microvasculature in coronary heart disease [26], as well as in characterizing cancer tumor microvessel structure [4,14].

The fractal dimensions derived for our networks ranged from 1.33 to 1.4202. Other reports of fractal dimension in other microvascular networks have ranged from 1.3 to 1.8 [30]. The usefulness of calculating the fractal dimension is two fold. First, it allowed for a quantitative comparison of the overall structural complexity of the arteriolar networks within the rat GM. Through this we found that our networks, in terms of their overall structure, varied only a small amount ($CV = 1.86\%$), thus confirming the relatively high geometric and topological similarity between networks discussed above. The second implication of calculating a fractal dimension will be its use in differentiating normal network structure from pathological conditions in future studies of the arteriolar networks of the rat GM.

2.5 Conclusion

We have provided a detailed quantitative analysis of the overall structure of rat GM arteriolar networks under baseline *in situ* conditions. These complex arteriolar networks followed similar geometric and topological patterns (i.e., Horton's laws) as the smaller terminal arteriolar networks of other skeletal muscle preparations. Ultimately, this study provides ideal geometric and topological parameters for use in theoretical studies of hemodynamics and blood flow regulation in complete/large microvascular networks with wide ranges of diameters and lengths.

2.6 References:

1. Al-Khazraji BK, Novielli NM, Goldman D, Medeiros PJ, Jackson DN. A simple "streak length method" for quantifying and characterizing red blood cell velocity profiles and blood flow in rat skeletal muscle arterioles. *Microcirculation* **19**: 327-335, 2012.
2. Al-Khazraji BK, Saleem A, Goldman D, Jackson DN. From one generation to the next: a comprehensive account of sympathetic receptor control in branching arteriolar trees. *J Physiol* **593**: 3093-3108, 2015.
3. Armstrong RB, Phelps RO. Muscle fiber type composition of the rat hindlimb. *Am J Anat* **171**: 259-272, 1984.
4. Baish JW, Jain RK. Fractals and cancer. *Cancer research* **60**: 3683-3688, 2000.
5. Bassingthwaighte JB. Fractal Vascular Growth Patterns. *Acta Stereol* **11**: 305-319, 1992.
6. Bassingthwaighte JB, King RB, Roger SA. Fractal nature of regional myocardial blood flow heterogeneity. *Circulation Research* **65**: 578-590, 1989.
7. Bearden SE. Effect of aging on the structure and function of skeletal muscle microvascular networks. *Microcirculation* **13**: 279-288, 2006.
8. Bearden SE, Payne GW, Chisty A, Segal SS. Arteriolar network architecture and vasomotor function with ageing in mouse gluteus maximus muscle. *J Physiol* **561**: 535-545, 2004.
9. Di Ieva A, Grizzi F, Ceva-Grimaldi G, Russo C, Gaetani P, Aimar E, Levi D, Pisano P, Tancioni F, Nicola G, Tschabitscher M, Dioguardi N, Baena RRY. Fractal dimension as a quantitor of the microvasculature of normal and adenomatous pituitary tissue. *J Anat* **211**: 673-680, 2007.
10. Ellsworth ML, Liu A, Dawant B, Popel AS, Pittman RN. Analysis of vascular pattern and dimensions in arteriolar networks of the retractor muscle in young hamsters. *Microvasc Res* **34**: 168-183, 1987.
11. Engelson ET, Skalak TC, Schmid-Schonbein GW. The microvasculature in skeletal muscle. I. Arteriolar network in rat spinotrapezius muscle. *Microvasc Res* **30**: 29-44, 1985.
12. Evanson KW, Stone AJ, Samraj E, Benson T, Prisby R, Kluess HA. Influence of estradiol supplementation on neuropeptide Y neurotransmission in skeletal muscle arterioles of F344 rats. *Am J Physiol Regul Integr Comp Physiol* **303**: R651-657, 2012.
13. Gan RZ, Tian Y, Yen RT, Kassab GS. Morphometry of the dog pulmonary venous tree. *J Appl Physiol (1985)* **75**: 432-440, 1993.

14. Gazit Y, Baish JW, Safabakhsh N, Leunig M, Baxter LT, Jain RK. Fractal characteristics of tumor vascular architecture during tumor growth and regression. *Microcirculation* **4**: 395-402, 1997.
15. Herman P, Kocsis L, Eke A. Fractal branching pattern in the pial vasculature in the cat. *J Cereb Blood Flow Metab* **21**: 741-753, 2001.
16. Horton RE. Erosional Development of Streams and Their Drainage Basins - Hydrophysical Approach to Quantitative Morphology. *Geol Soc Am Bull* **56**: 275-370, 1945.
17. Jackson DN, Moore AW, Segal SS. Blunting of rapid onset vasodilatation and blood flow restriction in arterioles of exercising skeletal muscle with ageing in male mice. *J Physiol* **588**: 2269-2282, 2010.
18. Karperien A, Ahammer H, Jelinek HF. Quantitating the subtleties of microglial morphology with fractal analysis. *Front Cell Neurosci* **7**: 3, 2013.
19. Kassab GS, Lin DH, Fung Y. Morphometry of pig coronary venous system. *Am J Physiol-Heart C* **267**: H2100-H2113, 1994.
20. Kassab GS, Rider CA, Tang NJ, Fung Y-C. Morphometry of pig coronary arterial trees. *Am J Physiol-Heart C* **265**: H350-H365, 1993.
21. Knoll A, Schmidt S, Chapman M, Wiley D, Bulgrin J, Blank J, Kirchner L. A comparison of two controlled-release delivery systems for the delivery of amiloride to control angiogenesis. *Microvascular research* **58**: 1-9, 1999.
22. Koller A, Dawant B, Liu A, Popel AS, Johnson PC. Quantitative analysis of arteriolar network architecture in cat sartorius muscle. *Am J Physiol* **253**: H154-164, 1987.
23. Lapi D, Marchiafava PL, Colantuoni A. Geometric characteristics of arterial network of rat pial microcirculation. *J Vasc Res* **45**: 69-77, 2008.
24. Less JR, Skalak TC, Sevick EM, Jain RK. Microvascular Architecture in a Mammary-Carcinoma - Branching Patterns and Vessel Dimensions. *Cancer Research* **51**: 265-273, 1991.
25. Liebovitch LS, Toth T. A Fast Algorithm to Determine Fractal Dimensions by Box Counting. *Phys Lett A* **141**: 386-390, 1989.
26. Liew G, Mitchell P, Rohtchina E, Wong TY, Hsu W, Lee ML, Wainwright A, Wang JJ. Fractal analysis of retinal microvasculature and coronary heart disease mortality. *European heart journal* **32**: 422-429, 2011.

27. Lucchese A, Gentile E, Capone G, De Vico G, Serpico R, Landini G. Fractal analysis of mucosal microvascular patterns in oral lichen planus: a preliminary study. *Oral surgery, oral medicine, oral pathology and oral radiology* **120**: 609-615, 2015.
28. Lucchese A, Gentile E, Capone G, De Vico G, Serpico R, Landini G. Fractal analysis of mucosal microvascular patterns in oral lichen planus: a preliminary study. *Oral Surg Oral Med Oral Pathol Oral Radiol* **120**: 609-615, 2015.
29. Mancardi D, Varetto G, Bucci E, Maniero F, Guiot C. Fractal parameters and vascular networks: facts & artifacts. *Theoretical Biology and Medical Modelling* **5**: 1, 2008.
30. Masters BR. Fractal Analysis of Normal Human Retinal Blood Vessels. *Fractals* **2**: 103-110, 1994.
31. Masters BR. Fractal analysis of the vascular tree in the human retina. *Annu Rev Biomed Eng* **6**: 427-452, 2004.
32. Moore AW, Bearden SE, Segal SS. Regional activation of rapid onset vasodilatation in mouse skeletal muscle: regulation through alpha-adrenoreceptors. *J Physiol* **588**: 3321-3331, 2010.
33. Popel AS, Johnson PC. Microcirculation and Hemorheology. *Annu Rev Fluid Mech* **37**: 43-69, 2005.
34. Pries AR, Secomb TW. Modeling structural adaptation of microcirculation. *Microcirculation* **15**: 753-764, 2008.
35. Pries AR, Secomb TW, Gaehtgens P. Relationship between structural and hemodynamic heterogeneity in microvascular networks. *Am J Physiol* **270**: H545-553, 1996.
36. Pries AR, Secomb TW, Gaehtgens P, Gross JF. Blood flow in microvascular networks. Experiments and simulation. *Circ Res* **67**: 826-834, 1990.
37. Schneider CA, Rasband WS, Eliceiri KW. NIH Image to ImageJ: 25 years of image analysis. *Nat Methods* **9**: 671-675, 2012.
38. Torres Filho IP, Cyrino FZ, Popel AS, Bouskela E, Johnson PC. Morphometric analysis of the anastomosing arteriolar network in cat sartorius muscle. *Int J Microcirc Clin Exp* **14**: 3-13, 1994.
39. Turcotte DL, Pelletier JD, Newman WI. Networks with side branching in biology. *Journal of theoretical biology* **193**: 577-592, 1998.

40. VanBavel E, Spaan J. Branching patterns in the porcine coronary arterial tree. Estimation of flow heterogeneity. *Circulation research* **71**: 1200-1212, 1992.
41. Xu LX, Holmes KR, Moore B, Chen MM, Arkin H. Microvascular architecture within the pig kidney cortex. *Microvasc Res* **47**: 293-307, 1994.

Chapter 3

Hemodynamic analysis of arteriolar networks in the rat gluteus maximus muscle

This chapter is in preparation to be submitted to the journal *Microcirculation* in September 2016.

3.1 Introduction

Theoretical blood flow modeling enables comprehensive analysis of hemodynamics of microvascular networks [23]. Often, microvascular networks exhibit high degrees of geometric and topological heterogeneity with regards to the distribution of the diameters, lengths, inter-connections, and flow pathways of the vessels forming the network [15,17]. Thus, a principal component of any computational study of network hemodynamics is to precisely define the network structure in terms of its geometric and topological organization [19].

Recently, we have provided detailed geometric and topological data describing the arteriolar network structure of the rat gluteus maximus muscle [1]. The data was collected *in vivo* using intravital videomicroscopy (IVVM), capturing the geometry and topology of the network under native baseline conditions. Our approach represents a marked improvement upon many previous studies of skeletal muscle arteriolar networks, both in terms of the technique in obtaining data as well as in the size and complexity of the networks. For example, previous studies describing microvascular geometry/topology have used vascular casting methods, requiring perfusion of vasodilatory agents and fixatives in an effort to visualize microvascular networks [4,5]. However, data captured under such conditions will vary from baseline conditions, especially with regards to diameters (due to the infusion of vasodilatory agents), bifurcation angles (evidence for change in angle with change in flow, which would change under maximal dilation [6]), and hemodynamics (blood flow, RBC distribution, resistance would all change under maximum diameters). Additionally, detailed analysis of skeletal muscle arteriolar network geometry and topology is often limited to the distal portions of networks (terminal arteriolar branches).

Therefore, the objective of this current study is to use recently collected *in situ* structural data as inputs into a computational blood flow model in order to assess the functional behavior of the arteriolar networks of the rat GM in terms of their hemodynamics. We assessed the variability of blood flow rates and hematocrit (discharge and tube) distribution within and between networks in order to measure the level of heterogeneity

within and between networks. Additionally, we sought to identify a network that may serve as a “mean” arteriolar network for future theoretical studies of skeletal muscle hemodynamics and blood flow regulation.

3.2 Materials and Methods

Data source:

In situ data were utilized from a previous study involving the measurement of geometric and topological properties of complete arteriolar networks ($n = 7$) of the rat GM preparation using IVVM [1]. Briefly, complete arteriolar networks arising from the inferior gluteal artery in the left GM of Sprague-Dawley rats were scanned under baseline conditions. Matlab (MathWorks Inc., Natick, MA, USA) was used to register individual IVVM frames together to create a photomontage of the complete arteriolar network. Approximately 500 overlapping frames were used to construct each photomontage. ImageJ (NIH, Bethesda, MD, USA)[22] was then used to measure the arteriolar network’s geometric properties (vessel diameter, lengths). A diameter measurement was made approximately every 150 μm along the length of each unbranched arteriolar segment, resulting in approximately 1500 sub-segments per network. Using Matlab, an automated centrifugal ordering algorithm (with order increasing at bifurcations when a daughter vessel had a diameter $<80\%$ of parent, or a bifurcation angle $>15^\circ$)[3] was applied to each network, resulting in arterioles ranging from 1st (proximal) to 9th (distal) order in 6 of the 7 networks studied. The remaining network resulted in centrifugal orders of 1 to 8.

Photomontages of arteriolar networks were converted into mathematical representations by constructing a scaled network of vessels made up of nodes connected by cylindrical sub-segments (Figure 10). Approximately 1500 discrete nodes were used to mathematically model each network, with an average distance of approximately 150 μm between each node, resulting in 145 to 279 vessel segments (and approximately 1500 sub-segments) per network.

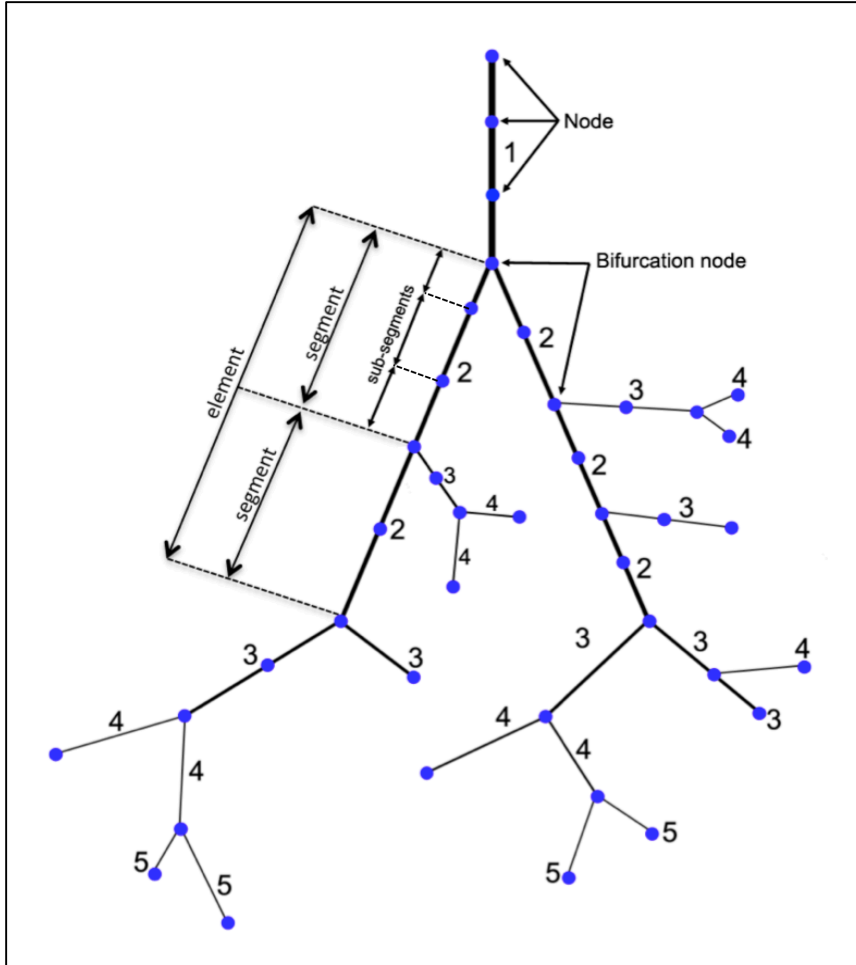


Figure 10: Schematic of node-segment representation in a simplified arteriolar network.

Arteriolar networks are discretized into cylindrical sub-segments connected through nodes. Sub-segments connected serially in between two bifurcation nodes are termed a segment. A number of segments connected serially within the same topological order are termed an element. Numbers indicate topological order.

Blood flow modelling:

Given information on diameters, lengths, and topological arrangement of all sub-segments in a network, a two-phase (RBC and plasma) continuum blood flow model developed in-house was used to calculate the steady-state distribution of total blood flow (Q) and hematocrit (Discharge Hematocrit H_D , Tube Hematocrit H_T) throughout each arteriolar network [8,9]. The model is governed by Poiseuille's law [14], and takes into

account the rheological behavior of blood through microvessels. Specifically, the Fahraeus effect (reduction of tube hematocrit with decreasing vessel diameter), phase-separation effect (uneven distribution of RBC and plasma at bifurcations), and the Fahreus-Lindqvist effect (reduction of viscosity with decreasing vessel diameter and hematocrit) are incorporated into the model based on empirical models derived from *in vivo* observations in the rat mesentery [16,20].

The mass conservation equations for overall blood and RBC volume flow into each node j are:

$$\sum_i Q_{ij} = 0 \quad \text{Eq. 1}$$

$$\sum_i H_{D_{ij}} Q_{ij} = 0 \quad \text{Eq. 2}$$

where each cylindrical vessel sub-segment ij is labeled by its nodes and the sums are over all nodes i connected to node j . The flow (Q) in sub-segment ij is given by the pressure difference across the sub-segment ij , divided by the hydrodynamic (Poiseuille) resistance of that sub-segment. Expressed mathematically:

$$Q_{ij} = \frac{(p_i - p_j)}{R_{ij}} \quad \text{Eq. 3}$$

$$R_{ij} = \frac{8\eta_{pl}\eta_{rel}L}{\pi r^4} \quad \text{Eq. 4}$$

where η_{pl} is the viscosity of plasma, η_{rel} is the apparent viscosity of blood (relative to plasma viscosity), L is the length of the vessel sub-segment, and r is the radius of the sub-segment.

Due to the non-linear rheological effects included in the model, solutions to the governing flow and hematocrit equations are solved alternately until satisfactory convergence occurs (error tolerance set to 10^{-11}).

Boundary Conditions:

The required boundary conditions necessary for solution of the model are the pressure (or flow) at all inflow and outflow nodes, as well as the discharge hematocrit at all inflow sub-segments.

The discharge hematocrit at the inlet sub-segment was assigned a value of 0.42 (typical value of blood sample hematocrit of Sprague-dawley rat [2]).

The pressure at the inlet node of the feed arteriole was fixed to a value of 80 mmHg. Outflow boundary pressure conditions are generally not known and difficult to measure, and therefore must be estimated. Since network flow resistance and blood flow distribution were of primary interest, the total blood flow into each network was set to match experimentally measured values in similar arteriolar branching trees of the rat GM based on the empirically derived equation [2]:

$$Q = 10^{-3.43} D^{2.63} \quad \text{Eq.5}$$

where D is the internal luminal diameter of the arteriole. Next, a least-squares approach was used that finds outflow pressures by minimizing the deviation of wall shear stresses (WSS) in all sub-segments and pressures at all nodes from given target values [7]. This approach was modified by performing a second set of iterations to estimate the target shear stress needed to match total blood flow and setting the target pressure to one-half the mean pressure in the network after each iteration [10,21].

Effective Network Resistance:

For a network with a single inlet and uniform pressure at all outlets, overall flow resistance (\mathcal{R}_{tot}) can be estimated as:

$$\mathcal{R}_{tot} = \frac{\Delta P}{Q_{tot}} \quad \text{Eq. 6}$$

where ΔP is the total pressure drop across the network and Q_{tot} is the total flow through the network.

However, this approach cannot be used with variable outlet pressures, as is the case for the current approach used in this study for approximating outflow boundary conditions. Therefore, we assume the work to pump blood through the network can be expressed as:

$$W = Q_{tot} \overline{\Delta P} \quad \text{Eq. 7}$$

where $\overline{\Delta P}$ is an effective mean pressure drop across the network, and use the fact that:

$$W = \sum_{outlets} Q_i \Delta P_i \quad \text{Eq. 8}$$

where ΔP_i is the pressure drop between the inlet node and the outlet node connected to sub-segment i . Then, based on the definition of \mathcal{R}_{tot} in Eq.6, the effective network resistance can be estimated as:

$$\overline{\mathcal{R}_{tot}} = \frac{1}{Q_{tot}^2} \sum_{outlets} Q_i \Delta P_i \quad \text{Eq. 9}$$

Statistical Analyses:

Experimental data are presented as mean \pm SEM, unless otherwise stated. Data were analyzed using Prism software (version 6.0g, GraphPad Software Inc., La Jolla, CA, USA) and differences were accepted as significantly different at $p < 0.05$. One-way ANOVA was used to test for differences between mean blood flow of each network and topological orders, as well as between mean blood flow at terminal segments for each network. Non-linear regression (exponential decay) was performed to evaluate the correlation between mean blood flow of all networks and topological order. Linear regression was performed to evaluate the correlation between mean hematocrit (discharge and tube) of all networks and topological order. The coefficient of variability (standard

deviation divided by the mean) was used to characterize the variation of mean blood flow and hematocrit with respect to topological order. The inter-network variability of the mean blood flow, $[CV(Q_{\text{mean},i})]$, or mean hematocrit, $[CV(H_{D\text{mean},i})]$ and $[CV(H_{T\text{mean},i})]$, was calculated by determining the mean blood flow ($Q_{\text{mean},i}$) or mean hematocrit ($H_{D\text{mean},i}$), ($H_{T\text{mean},i}$) of a given order for each network i ($i = 1$ to 7), followed by calculating the corresponding coefficient of variability. Similarly, the average blood flow intra-network variability, $[\text{mean } CV_i(Q_{\text{mean},i})]$, was calculated by first determining the coefficient of variability for the mean blood flow ($Q_{\text{mean},i}$) of a given order for each network i ($i = 1$ to 7), $CV_i(Q_{\text{mean},i})$, followed by averaging these CV_i values over the population of networks ($n = 7$ networks) for each topological order.

3.3 Results

Table 7 describes some of the basic geometric and topological characteristics of each network considered. Each network was fed by a single inlet vessel (inferior gluteal artery), progressed through 8 to 9 orders of bifurcations, and terminated with an average of 109 ± 22 outlet (terminal) arterioles. The average pressure drop from the feed to the terminal node was 18 ± 6.15 mmHg, in agreement with a previous result for similar arteriolar networks [3].

Table 7: Characteristics of the arteriolar network models.

Network	No. of orders	Total No. of nodes	No. of bifurcation nodes	No. of Segments	No. of inflow segments	No. of outflow segments	Average pressure drop at outlets
1	9	1644	236	235	1	118	28.83
2	9	1657	212	211	1	107	10.71
3	9	1222	180	179	1	90	19.77
4	9	1629	236	235	1	118	12.61
5	9	1511	238	237	1	119	14.02
6	8	1178	146	145	1	73	20.11
7	9	1727	280	279	1	140	20.09
Mean	8.89 ± 0.14	1509 ± 83	218 ± 17	217 ± 17	1	109 ± 8	18 ± 2.33

Data presented as mean ± SEM (n=7 animals). Pressure drop given in mmHg.

Mean blood flow through each vessel segment of all networks exponentially decayed (Exponential decay fit: $R^2 = 0.99$) with increasing topological order (1A to 9A) (Figure 11). The inter-network coefficient of variation (a measure of variability of blood flow distribution between networks) ranged from 3.43% at 1A to 35.94% at 9A, with a maximum variation of 45.51% and 70.54% occurring at orders 6A and 7A respectively.

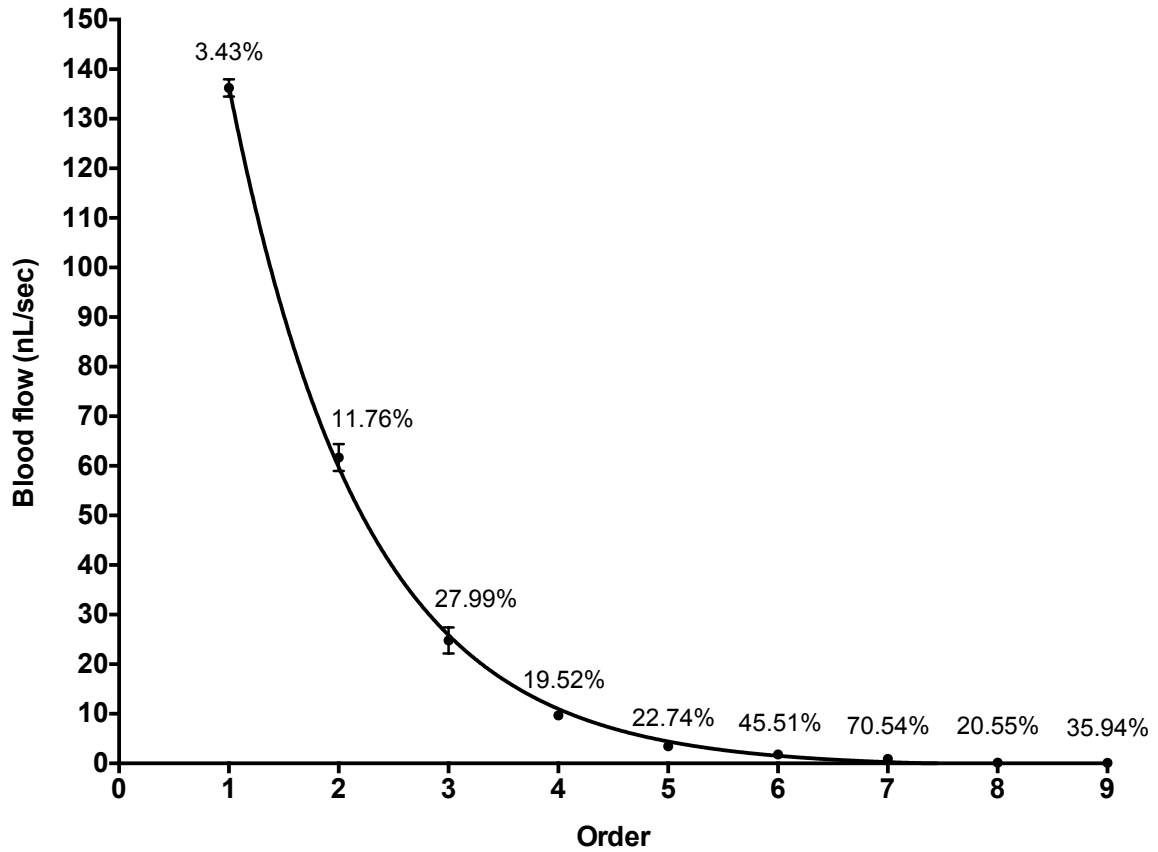


Figure 11: Relationship between mean blood flow and topological order.

Mean blood flow through each vessel segment of all networks exponentially decayed (Exponential decay fit: $R^2 = 0.99$) with increasing topological order. Inter-network CVs are labeled above each data point. Data points are mean \pm SEM ($n = 7$ networks).

Log-Log plots between blood flow and diameter exhibited a strong linear correlation for each network (Linear Regression fit: $R^2 > 0.90$, $p < 0.001$) (Figure 12). The slopes of the linear regression lines ranged from 2.801 to 3.104, with a mean \pm SD of 2.966 ± 0.11 (Table 8). The slope of the linear regression line when data from all networks were pooled into one plot was 2.907 (Linear Regression fit: $R^2 = 0.89$, $p < 0.001$).

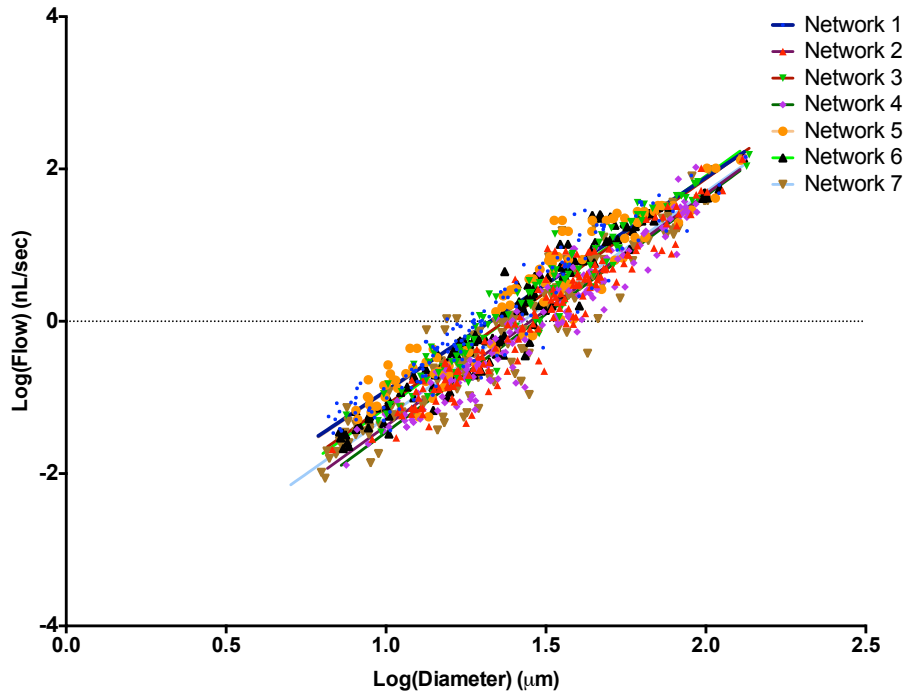


Figure 12: Log-log relationship between blood flow and arteriolar diameter.

Log-Log plots between blood flow and diameter exhibited a strong linear correlation for each network (Linear Regression fit: $R^2 > 0.90$, $p < 0.001$). The slopes of the linear regression lines ranged from 2.801 to 3.104, with a mean \pm SD of 2.966 ± 0.11 . The slope of the linear regression line when data from all networks were pooled into one plot was 2.907 ($R^2 = 0.89$, $p < 0.001$).

Table 8: Relationship between blood flow and arteriolar diameter.

Network	Linear Regression equation	R^2	95% confidence interval of slope
1	$\log(Q) = 2.801 \cdot \log(D) - 3.714$	0.91	2.757 to 2.845
2	$\log(Q) = 3.043 \cdot \log(D) - 4.417$	0.92	2.998 to 3.087
3	$\log(Q) = 2.973 \cdot \log(D) - 4.076$	0.94	2.929 to 3.016
4	$\log(Q) = 3.104 \cdot \log(D) - 4.561$	0.90	3.055 to 3.153
5	$\log(Q) = 2.805 \cdot \log(D) - 3.732$	0.90	2.751 to 2.858
6	$\log(Q) = 3.044 \cdot \log(D) - 4.179$	0.93	3.003 to 3.085
7	$\log(Q) = 2.965 \cdot \log(D) - 4.229$	0.90	2.919 to 3.011
Pooled	$\log(Q) = 2.907 \cdot \log(D) - 4.061$	0.89	2.887 to 2.927

Q and D are flow (nL/sec) and diameter (μm). Linear regression slopes significant at $p < 0.0001$.

The mean blood flow through each topological order of each network did not differ significantly across networks (One way ANOVA, $p = ns$) (Figure 13A and 13B). The average intra-network coefficient of variation (an average measure of variability of blood flow distribution within each network) ranged from 3% at order 1A to 118% at 9A, with a peak in average variability of 164% and 188% occurring at orders 6A and 7A respectively.

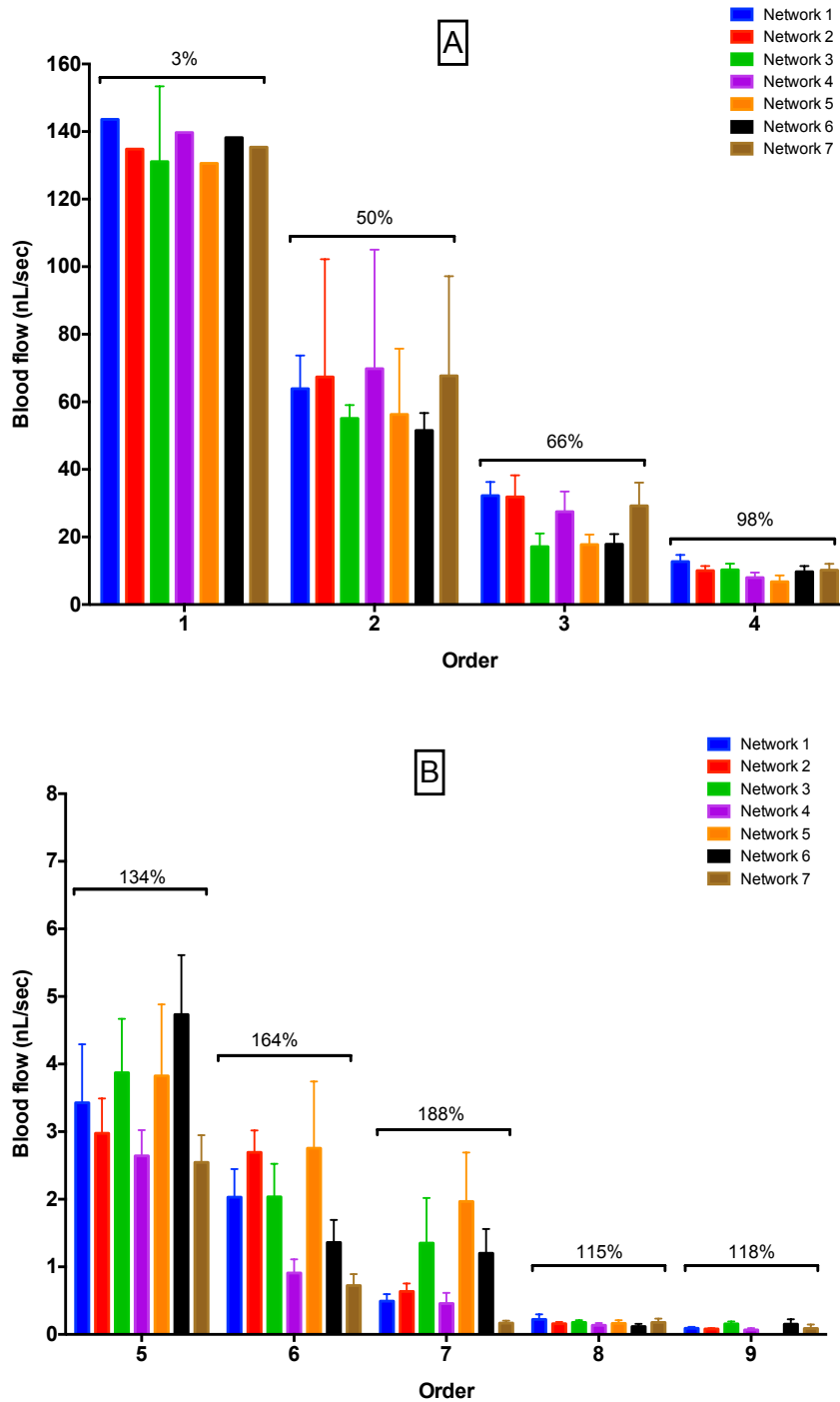


Figure 13 (A&B): Relationship of mean blood flow between networks at orders 1-4 (A) and 5-9 (B), with average intra-network variability expressed above each group. The mean blood flow at each topological order of each network did not differ significantly across networks (One way ANOVA, $p = ns$). The average intra-network coefficient of variation ranged from 3% at order 1A to 118% at 9A, with a peak in average variability of 164% and 188% occurring at orders 6A and 7A respectively. Data presented as mean \pm SEM ($n = 7$ networks).

The mean blood flow through each outflow (terminal) segment did not differ significantly between networks (One way ANOVA, $p = ns$) (Figure 14). However, the variability in flow through terminal segments of each network was extremely high, with CV's ranging from 184.30% to 426.21%, with an average CV of 260.51%.

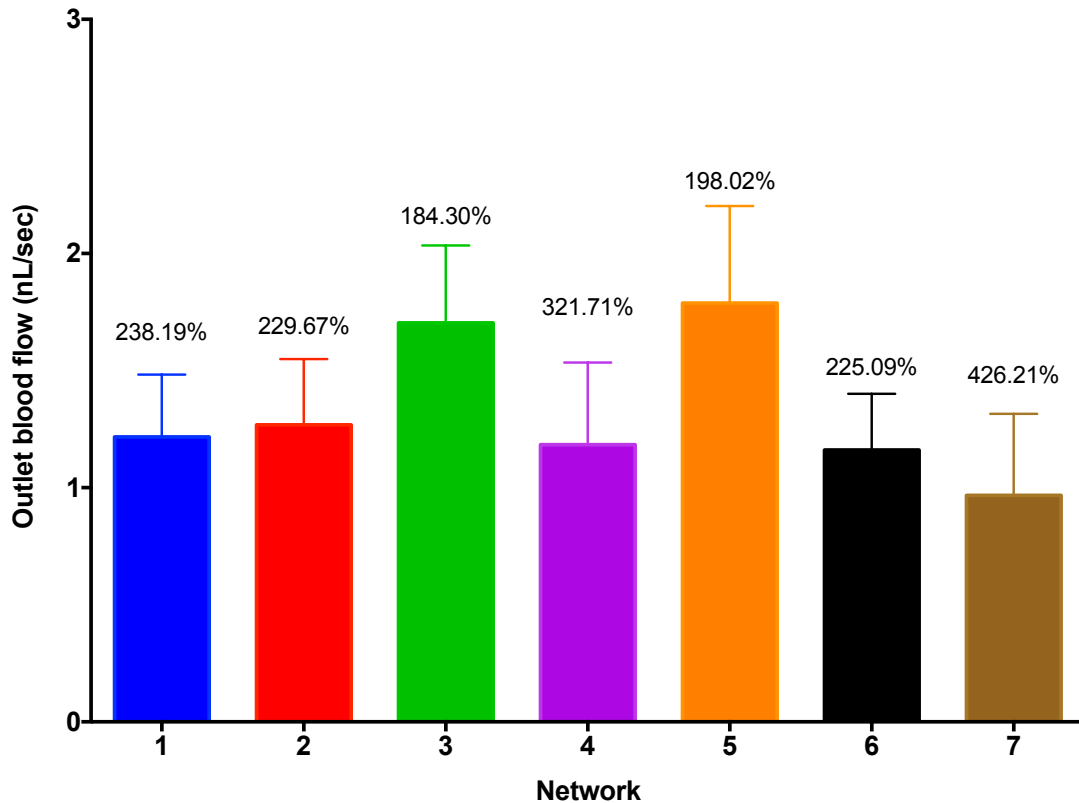


Figure 14: Relationship of mean outlet blood flow between networks.

The mean blood flow through each outflow (terminal) segment did not differ significantly between networks (One way ANOVA, $p = ns$). However, the variability in flow through terminal segments of each network was extremely high, with CV's ranging from 184.30% to 426.21%, with an average CV of 260.51%. Data presented as mean \pm SEM.

Mean discharge and tube hematocrit of all networks exhibited a linearly decreasing trend with increasing topological order (Linear regression: $R^2 = 0.9638$ for H_D , $R^2 = 0.9762$ for H_T) (Figure 15). The inter-network coefficient of variation of hematocrit increased with increasing topological order for both discharge (1A: 0.05%, 9A: 14.51%) and tube

hematocrit (1A: 0.26%, 9A: 15.57%), with the highest variation occurring at the distal orders (6A to 9A).

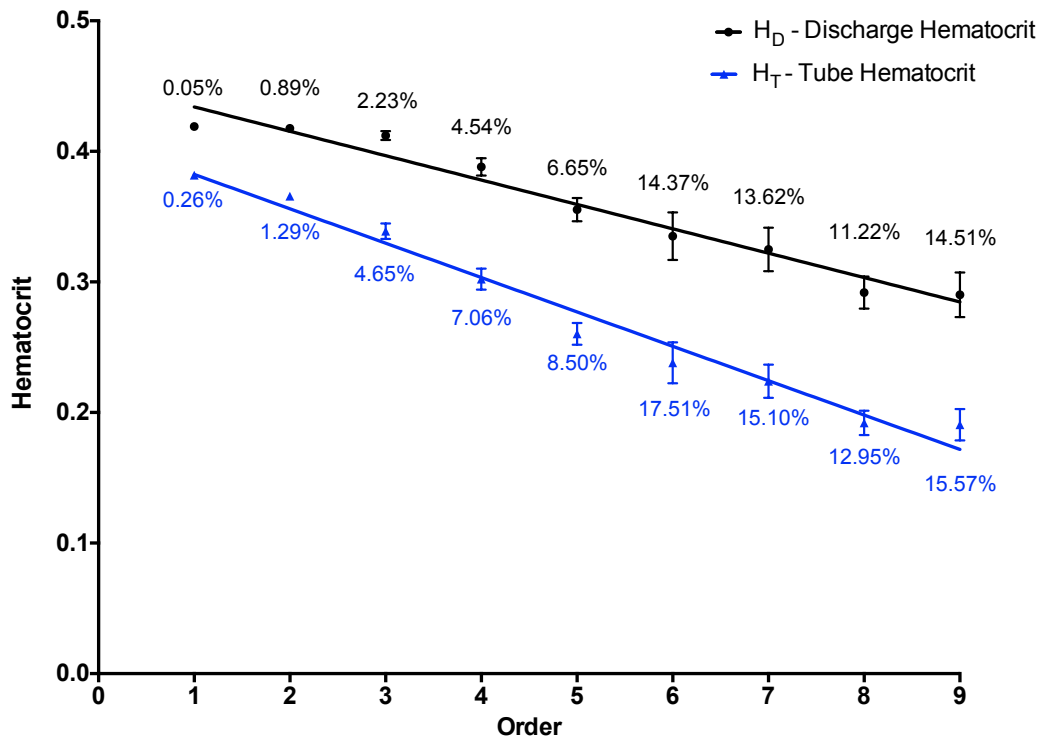


Figure 15: Relationship between mean hematocrit of all networks and order.

Mean discharge and tube hematocrit of all networks exhibited a linearly decreasing trend with increasing topological order (Linear regression: $R^2 = 0.9638$ for H_D, $R^2 = 0.9762$ for H_T). The inter-network coefficient of variation of hematocrit increased with increasing topological order for both discharge (1A: 0.05%, 9A: 14.51%) and tube hematocrit (1A: 0.26%, 9A: 15.57%), with the highest variation occurring at the distal orders (6A to 9A). Data presented as mean \pm SEM.

The effective network resistance (\mathcal{R}_{tot}) was compared between all networks (Figure 16). \mathcal{R}_{tot} ranged from 1196.09 to 3508.85 PRU, with an overall mean \pm SD of 2198.01 \pm 309.11.

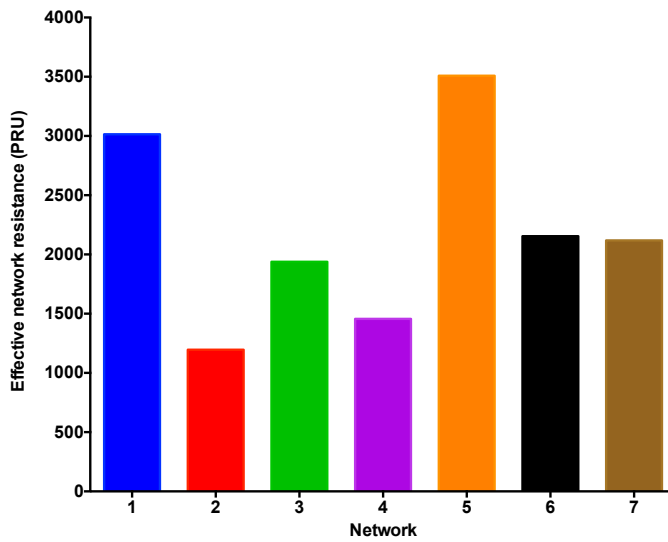


Figure 16: Comparison of effective network resistance (\mathcal{R}_{tot}) between networks.

\mathcal{R}_{tot} ranged from 1196.09 to 3508.85 PRU, with an overall mean \pm SEM of 2198.01 \pm 309.11. \mathcal{R}_{tot} presented in PRU units (mmHg*ml/min).

Finally, from the 7 networks analyzed, a “mean” (i.e. most representative) network is chosen based on its structural (geometric and topological) and hemodynamic properties closely aligning with mean values. Towards this goal, network 7 is suggested (Table 9).

Table 9: Comparison of structural and hemodynamic properties between mean of all networks and network 7

Property	Mean of all networks	Network 7	Percent deviation
Structural			
No. of orders	8.89	9	1.22%
R _D	1.4016	1.4372	2.48%
R _L	1.4896	1.5413	3.35%
R _B	2.1661	2.2360	3.24%
Fractal Dimension	1.3844	1.4202	2.52%
Hemodynamic			
Average Pressure Drop (mmHg)	18.02	20.09	10.30%
Effective Network Resistance (PRU)	2198.01	2118.98	-3.73%
Slope of log(Q) vs log(D)	2.907	2.965	1.96%

Percent deviation calculated as: $(\text{Network 7} - \text{Mean of all networks}) / (\text{Network 7}) * 100\%$. Structural data taken from ref [1].

3.4 Discussion

In an effort to determine the functional (hemodynamic) characteristics of arteriolar networks within locomotive skeletal muscle, we used recently reported baseline *in situ* arteriolar network geometry and topology from rat gluteus maximus muscle as inputs for our computational blood flow model. Using our computational blood flow model, and building upon previous methods for estimating unknown boundary conditions, we analyzed the distribution of blood flow and hematocrit through complex arteriolar networks in skeletal muscle, as well as the associated variability exhibited between and within networks.

Based on our simulations, arteriolar networks of the rat GM exhibit strong inter-network homology with respect to blood flow as a function of topological order. In all networks, the mean blood flow decreased exponentially with increasing topological order, with no significant difference in mean blood flow between networks at all topological orders. Furthermore, the inter-network variability of mean blood flow at each topological order (~3 to 36%) was consistently much lower than the corresponding intra-network variability (~50 to 118%). Therefore, although the distribution of blood flow with respect to topological order may be highly heterogeneous within networks, this intra-network variability is likely a consistent feature across all networks leading to relatively homogenous distributions of inter-network blood flow.

Similarly, mean discharge and tube hematocrit were found to decrease at progressively higher topological orders, with a correspondingly slight increase in inter-network heterogeneity at orders 6A to 9A. The fall in tube hematocrit (RBC fraction of daughter vessels originating from a “reservoir” or “discharge” parent vessel) is explained by the Fahraeus effect. This effect is in part due to the higher velocity of RBCs relative to plasma. This difference in velocity is caused by the axial migration of RBCs towards the center of the vessel, creating a cell-free (plasma) layer near the wall of the vessel. This difference in velocity between RBC and plasma leads to a higher volume concentration of RBC within the daughter (narrower) vessels in comparison to the parent (larger) vessel. The increase in variability reflects an increase in spatial heterogeneity of RBC supply, possibly leading to an increase in heterogeneity of oxygen transport as well. The increase in heterogeneity observed for both blood flow and hematocrit is likely related to the unsymmetrical nature of the arteriolar networks, which possess flow paths to outflow segments of varying diameters, lengths, and number of bifurcations. In analyzing the distribution of vessel diameters and lengths, we observed the highest levels of intra-network heterogeneity at the distal orders, especially 6A to 8A [1].

The log-log relationships of blood flow and diameter further reinforce the observed homology exhibited between networks, as reflected by the small variances in slopes of linear regression lines. Our simulations indicate a close agreement to Murray’s law [13], a hypothesis regarding the optimal structural design of microvascular networks. In his

classic work, Murray deduced that based on minimizing the cardiac and metabolic work necessary to deliver and maintain blood and its encompassing vessels, an optimal network structure is obtained when blood flow is proportional to vessel diameter cubed, which for Poiseuille flow, implies a uniform wall shear stress throughout the network. Evidence supporting Murray's law has been reported in arterial as well as arteriolar networks in several types of tissues of both humans and animals [12,24-26]. However, based on observations in veins and venular networks, much lower WSS has been reported in comparison to the arterial/arteriolar sides [12], implying Murray's law may only apply to the arterial/arteriolar side and promoting an alternative theory on microvascular network design based on maintaining local WSS at a set point that is dependent on local transmural pressure [18].

Our criteria for selecting a "mean" network was based upon identifying a network that aligned closely with the mean values of relevant geometric/topological as well as hemodynamic values. The properties chosen as most relevant were: the number of topological orders, Horton's Ratios (Bifurcation, Diameter, and Length Ratio), fractal dimension, the average pressure drop throughout the network, the total resistance of the network, and the slope of the flow-diameter relationship. Based upon this criteria, we identified network #7 as the network most closely matching mean values. Although this set of criteria includes some of the most relevant geometric and hemodynamic variables, not all properties are considered and thus some values may deviate significantly from the mean. For example, network #7 was found to have the highest number of total vessel segments as well as terminal outflow segments.

Poiseuille flow, which predicts parabolic shapes of velocity profiles, was assumed in our computational model. However, a previous study from our laboratory where RBC velocity profiles were experimentally measured demonstrated a blunting of the velocity profile with decreasing diameter [2]. Thus, although the computational model was validated against experimental measurements of blood and RBC flow, a question remains whether Poiseuille flow is an appropriate assumption of the model, especially with regards to the smallest (~15-30 μm) vessels of the arteriolar network. This study would also be

enhanced by the addition of experimentally measured values of pressure, shear-stress, and hematocrit at the inlet as well as some of the outlet vessels.

The results presented within this study are based on *in situ* measurements of arteriolar network structure in skeletal muscle, and thus do not include the other components of the microcirculation, namely the capillaries and venules. Thus, in order to extend the results of this study into processes fundamental to the function of skeletal muscle such as oxygen transport or electrical communication between microvessels, data on the geometry and topology of capillary and venular networks are necessary.

3.5 Conclusion

We have assessed the blood flow and hematocrit distribution through complete arteriolar networks using baseline *in situ* data of the overall geometric and topological structure of the rat GM arteriolar networks. Blood flow and hematocrit both decreased with increasing topological order, and were much more heterogeneously distributed within networks than across networks. Ultimately, this study relates the structure of large arteriolar networks to their function, and is a step towards building an ideal locomotive skeletal muscle microcirculatory network to facilitate future microvascular research.

3.6 References

1. Al Tarhuni M, Goldman D, Jackson DN. Comprehensive in situ analysis of arteriolar network geometry and topology in rat gluteus maximus muscle. *Microcirculation*, 2016.
2. Al-Khazraji BK, Novielli NM, Goldman D, Medeiros PJ, Jackson DN. A simple "streak length method" for quantifying and characterizing red blood cell velocity profiles and blood flow in rat skeletal muscle arterioles. *Microcirculation* **19**: 327-335, 2012.
3. Al-Khazraji BK, Saleem A, Goldman D, Jackson DN. From one generation to the next: a comprehensive account of sympathetic receptor control in branching arteriolar trees. *J Physiol* **593**: 3093-3108, 2015.
4. Ellsworth M, Liu A, Dawant B, Popel A, Pittman R. Analysis of vascular pattern and dimensions in arteriolar networks of the retractor muscle in young hamsters. *Microvascular research* **34**: 168-183, 1987.
5. Engelson ET, Skalak TC, Schmid-Schönbein GW. The microvasculature in skeletal muscle: I. Arteriolar network in rat spinotrapezius muscle. *Microvascular research* **30**: 29-44, 1985.
6. Frame MD, Sarelius IH. Arteriolar bifurcation angles vary with position and when flow is changed. *Microvasc Res* **46**: 190-205, 1993.
7. Fry BC, Lee J, Smith NP, Secomb TW. Estimation of blood flow rates in large microvascular networks. *Microcirculation* **19**: 530-538, 2012.
8. Goldman D, Popel AS. A computational study of the effect of capillary network anastomoses and tortuosity on oxygen transport. *Journal of theoretical biology* **206**: 181-194, 2000.
9. Goldman D, Popel AS. A computational study of the effect of vasomotion on oxygen transport from capillary networks. *Journal of theoretical biology* **209**: 189-199, 2001.
10. Goldman D, Saleem AH, Al-Khazraji BK, Jackson DN. Estimating Blood Flow in Skeletal Muscle Arteriolar Trees Reconstructed from In Vivo Data. *The FASEB Journal* **30**: 947.942-947.942, 2016.
11. Lapi D, Marchiafava PL, Colantuoni A. Geometric characteristics of arterial network of rat pial microcirculation. *J Vasc Res* **45**: 69-77, 2008.
12. Mayrovitz HN, Roy J. Microvascular blood flow: evidence indicating a cubic dependence on arteriolar diameter. *Am J Physiol* **245**: H1031-H1038, 1983.

13. Murray CD. The physiological principle of minimum work I. The vascular system and the cost of blood volume. *Proceedings of the National Academy of Sciences* **12**: 207-214, 1926.
14. Poiseuille JLM. *Recherches sur les causes du mouvement du sang dans les veines* edn: impr. H. Tilliard, 1830.
15. Popel A. Network models of peripheral circulation. *Handbook of Bioengineering*: 20.21-20.24, 1987.
16. Pries A, Secomb T, Gessner T, Sperandio M, Gross J, Gaehtgens P. Resistance to blood flow in microvessels in vivo. *Circulation research* **75**: 904-915, 1994.
17. Pries AR, Secomb TW. Microcirculatory network structures and models. *Annals of biomedical engineering* **28**: 916-921, 2000.
18. Pries AR, Secomb TW, Gaehtgens P. Design principles of vascular beds. *Circulation Research* **77**: 1017-1023, 1995.
19. Pries AR, Secomb TW, Gaehtgens P. Relationship between structural and hemodynamic heterogeneity in microvascular networks. *Am J Physiol* **270**: H545-553, 1996.
20. Pries AR, Secomb TW, Gaehtgens P, Gross JF. Blood-Flow in Microvascular Networks - Experiments and Simulation. *Circulation Research* **67**: 826-834, 1990.
21. Saleem AH. Estimating Hemodynamics in Skeletal Muscle Arteriolar Networks Reconstructed From In Vivo Data. M.Sc. Thesis. University of Western Ontario, London, 2015.
22. Schneider CA, Rasband WS, Eliceiri KW. NIH Image to ImageJ: 25 years of image analysis. *Nat Methods* **9**: 671-675, 2012.
23. Secomb TW, Beard DA, Frisbee JC, Smith NP, Pries AR. The role of theoretical modeling in microcirculation research. *Microcirculation* **15**: 693-698, 2008.
24. Sherman TF, Popel AS, Koller A, Johnson PC. The cost of departure from optimal radii in microvascular networks. *Journal of theoretical biology* **136**: 245-265, 1989.
25. Zamir M, Medeiros J. Arterial branching in man and monkey. *The Journal of general physiology* **79**: 353-360, 1982.
26. Zamir M, Wrigley S, Langille B. Arterial bifurcations in the cardiovascular system of a rat. *The Journal of general physiology* **81**: 325-335, 1983.

Chapter 4

Contributions and Future Work

4.1 Contributions

This thesis presents novel findings on the morphology and hemodynamics of arteriolar networks that will contribute to better overall understanding of the microcirculation, especially within skeletal muscle. The overall “network” approach taken to study the morphology of arterioles within the rat gluteus maximus provides new insight and detailed quantitative descriptions of the arteriolar network structure, while placing an important emphasis on studying the network structure as a whole rather than an isolated number of branches/bifurcations or smaller terminal networks.

Overall, we have improved upon previous reports of skeletal muscle arteriolar network morphology in several regards, most importantly with the specific approach to imaging the microcirculation. The use of intravital video-microscopy to image the microvasculature enabled us to capture the geometry (diameter, lengths, bifurcation angles) and topology (inter-connections of vessels within a network) under native baseline conditions. This is a significant distinction from many earlier studies of microvascular morphology, which required maximal vasodilation of the vasculature prior to injection of fixative substances (gelatin, carbon particles, silicon rubber filling) for casting. Interpretation of data from casting studies are limited as the geometric data is collected under maximal vasodilatory state, where both the diameters [3], as well as the bifurcation angles, differ from resting baseline conditions [2]. Additionally, the use of the rat gluteus maximus (GM) preparation enables several improvements over other skeletal muscle preparations used in IVVM. The GM is common to all mammalian species of both sexes (as opposed to the cremaster, for example), and is recruited and activated during locomotion, which is an important function of skeletal muscle (as opposed to the cheek pouch retractor, for example). Direct investigation of the microvasculature of the rat GM is ideal due to the intrinsic anatomical layout of the microvasculature within the

GM (tree-like branching arteriolar network supplied by a single feed artery) combined with its relatively uniform thinness results in the microcirculation (arterioles, venules, and capillaries) being optimally positioned for complete imaging of the network within a single focal plane (with minor tunings of fine focus).

With our approach to imaging the microvasculature of the gluteus maximus of the rat, we were able to characterize the native geometry (diameter, lengths) and topology (interconnections of vessels within network) of complete arteriolar networks (feed to terminal arterioles) over a wider range of diameters (~130 to 10 μm) and topological orders (1 to 9) than previously done. We have shown that arteriolar networks of the rat GM obey Horton's laws, and the ratios (diameter, length, bifurcation) obtained were similar to previous reports in both skeletal muscle as well as non-skeletal muscle tissues.

Based upon our experimentally derived data on network structure, and in combination with previously collected experimental data of blood flow velocity profiles in similar arteriolar trees, we were able to characterize the functional behavior of the arteriolar networks of the GM with regards to its blood flow, resistance, and hematocrit distributions using theoretical blood flow modeling. We report that mean blood flow followed an exponentially decaying trend with increasing order, while hematocrit (discharge and tube) followed a linearly decreasing trend. The relatively low levels of inter-network geometric and topological heterogeneity observed between networks resulted in similarly low levels of inter-network heterogeneity of mean blood flow and hematocrit distribution between networks. Interestingly, log-log plots of blood flow vs diameters indicated that the blood flow within arteriolar networks of the rat GM is proportional to the diameter cubed, a relationship known as Murray's Law. The hemodynamic data presented provide a new perspective on skeletal muscle hemodynamics by evaluating inter-network and intra-network hemodynamic variability among complete skeletal muscle arteriolar networks.

4.2 Future Work

Although the arterioles play a fundamental role in the regulation and distribution of blood flow within tissue, they form only one “level” of the microcirculation. Complementary morphological and hemodynamic studies of the venular and capillary networks of the rat GM are the next logical step in the progression towards a full representation of the microcirculation of the rat GM. As previously discussed, the rat GM is perfectly suited for such future studies, as both the venules and capillaries are optimally positioned for IVVM imaging. Such microvascular models encompassing all three levels of the microcirculation (arterioles, capillaries, venules) have been obtained for the rat mesentery [4] as well as the rabbit omentum and human conjunctiva [1]; however, a similar model of skeletal muscle microvasculature has yet to be developed. The development of such a skeletal muscle model would present a powerful tool to microvascular researchers interested in understanding the relationship between experimentally observed changes of the microvascular geometry/topology and related changes in hemodynamics and function of the microvascular bed.

Additionally, the data presented herein will serve as valuable reference points for the healthy and baseline conditions of the arteriolar networks of the rat GM, and aid in future studies investigating the effects of pharmacological perturbations and/or pathological conditions on the microcirculation. Indeed, many conditions have been shown to lead to altered sensitivity of arterioles to alter their diameter in response to muscle contraction and SNS activation. Microvascular remodeling following vessel occlusion or ischemic conditions (reactive hyperemia) have also been reported. Therefore, the structural and functional data on the healthy rat GM, possibly including the fractal dimension, will serve as valuable controls for future studies of pathological conditions and may aid in identifying any structural and/or functional changes underlying disease conditions.

4.3 References

1. Fenton BM, Zweifach B. Microcirculatory model relating geometrical variation to changes in pressure and flow rate. *Annals of Biomedical Engineering* **9**: 303-321, 1981.
2. Frame MD, Sarelius IH. Arteriolar bifurcation angles vary with position and when flow is changed. *Microvasc Res* **46**: 190-205, 1993.
3. Koller A, Dawant B, Liu A, Popel AS, Johnson PC. Quantitative analysis of arteriolar network architecture in cat sartorius muscle. *Am J Physiol* **253**: H154-164, 1987.
4. Ley K, Pries A, Gaehtgens P. Topological structure of rat mesenteric microvessel networks. *Microvascular research* **32**: 315-332, 1986.
5. Pries AR, Secomb TW, Gaehtgens P. Design principles of vascular beds. *Circ Res* **77**: 1017-1023, 1995.

Appendix A – Figure Permissions

Rightslink® by Copyright Clearance Center



RightsLink®

Home

Account
Info

Help



KARGER

Title: Morphometric Analysis of the
Anastomosing Arteriolar
Network in Cat Sartorius Muscle

Author: Torres Filho I.P., Cyrino
F.Z.G.A., Popel A.S., et al

Publication: Journal of Vascular Research

Publisher: Karger Publishers

Date: Jul 1, 1994

Copyright © 1994, Karger Publishers

Order Completed

Thank you for your order.

This Agreement between mohammed k al tarhuni ("You") and Karger Publishers ("Karger Publishers") consists of your license details and the terms and conditions provided by Karger Publishers and Copyright Clearance Center.

Your confirmation email will contain your order number for future reference.

[Get the printable license.](#)

License Number	3923711055035
License date	Aug 07, 2016
Licensed Content Publisher	Karger Publishers
Licensed Content Publication	Journal of Vascular Research
Licensed Content Title	Morphometric Analysis of the Anastomosing Arteriolar Network in Cat Sartorius Muscle
Licensed copyright line	Copyright © 1994, Karger Publishers
Licensed Content Author	Torres Filho I.P., Cyrino F.Z.G.A., Popel A.S., et al
Licensed Content Date	Jul 1, 1994
Licensed Content Volume	14
Licensed Content Issue	1-2
Special issue or supplement	
Type of use	Thesis/Dissertation
Requestor type	student
Format	Print, Electronic
Portion	figures/tables/illustrations
Number of figures/tables/illustrations	1
Include Image file	no
Rights for	Main product
Duration of use	Life of current edition/presentation
Creation of copies for the disabled	no
With minor editing privileges	no
For distribution to	Worldwide
Lifetime unit quantity of new product	1
The requesting person/organization	Mohammed Al Tarhuni
Order reference number	
Title of your thesis / dissertation	Comprehensive topological, geometric, and hemodynamic analysis of rat gluteus maximus arteriolar networks
Expected completion date	Aug 2016

Rightslink® by Copyright Clearance Center

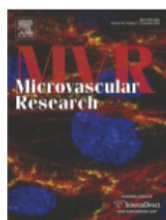


RightsLink®

Home

Account
Info

Help



Title: Topological structure of rat mesenteric microvessel networks

Author: K. Ley, A.R. Pries, P. Gaehtgens

Publication: Microvascular Research

Publisher: Elsevier

Date: November 1986

Copyright © 1986 Published by Elsevier Inc.

Order Completed

Thank you for your order.

This Agreement between mohammed k al tarhuni ("You") and Elsevier ("Elsevier") consists of your license details and the terms and conditions provided by Elsevier and Copyright Clearance Center.

Your confirmation email will contain your order number for future reference.

[Get the printable license.](#)

License Number	3923710127642
License date	Aug 07, 2016
Licensed Content Publisher	Elsevier
Licensed Content Publication	Microvascular Research
Licensed Content Title	Topological structure of rat mesenteric microvessel networks
Licensed Content Author	K. Ley, A.R. Pries, P. Gaehtgens
Licensed Content Date	November 1986
Licensed Content Volume	32
Licensed Content Issue	3
Licensed Content Pages	18
Type of Use	reuse in a thesis/dissertation
Portion	figures/tables/illustrations
Number of figures/tables/illustrations	1
Format	electronic
Are you the author of this Elsevier article?	No
Will you be translating?	No
Order reference number	
Original figure numbers	1
Title of your thesis/dissertation	Comprehensive topological, geometric, and hemodynamic analysis of rat gluteus maximus arteriolar networks
Expected completion date	Aug 2016
Estimated size (number of pages)	88
Elsevier VAT number	GB 494 6272 12
Requestor Location	mohammed k al tarhuni

Attn: mohammed k al tarhuni
Total 0.00 USD

[ORDER MORE](#)

[CLOSE WINDOW](#)

Rightslink® by Copyright Clearance Center



RightsLink®

[Home](#)[Account Info](#)[Help](#)

Title: Structural adaptation increases predicted perfusion capacity after vessel obstruction in arteriolar arcade network of pig skeletal muscle

Author: Gabriel Gruionu, James B. Hoying, Lucian G. Gruionu, M. Harold Laughlin, Timothy W. Secomb

Publication: Am J Physiol- Heart and Circulatory Physiology

Publisher: The American Physiological Society

Date: Jun 1, 2005

Copyright © 2005, Copyright © 2005 by the American Physiological Society

Permission Not Required

Permission is not required for this type of use.

[BACK](#)[CLOSE WINDOW](#)

Copyright © 2016 [Copyright Clearance Center, Inc.](#) All Rights Reserved. [Privacy statement.](#) [Terms and Conditions.](#) Comments? We would like to hear from you. E-mail us at customercare@copyright.com

Appendix B – Animal Use Protocol Approval

From: eSiriusWebServer
To: Dwayne Jackson
CC:
Date: 9/17/2015 3:08 PM
Subject: eSirius Notification - Annual Protocol Renewal APPROVED by the AUS 2012-018::3



2012-018::3:
AUP Number: 2012-018
AUP Title: Microvascular function in skeletal muscle
Yearly Renewal Date: 09/01/2015
The YEARLY RENEWAL to Animal Use Protocol (AUP) 2012-018 has been approved, and will be approved for one year following the above review date.

1. This AUP number must be indicated when ordering animals for this project.
2. Animals for other projects may not be ordered under this AUP number.
3. Purchases of animals other than through this system must be cleared through the ACVS office. Health certificates will be required.

REQUIREMENTS/COMMENTS

Please ensure that individual(s) performing procedures on live animals, as described in this protocol, are familiar with the contents of this document.

The holder of this Animal Use Protocol is responsible to ensure that all associated safety components (biosafety, radiation safety, general laboratory safety) comply with institutional safety standards and have received all necessary approvals. Please consult directly with your institutional safety officers.

Submitted by: Kinchlea, Will D
on behalf of the Animal Use Subcommittee

Curriculum Vitae

Name: Mohammed Al Tarhuni

Post-secondary Education and Degrees: The University of Western Ontario
London, Ontario, Canada
2009-2014 B.Sc. (Applied Mathematics, Medical Sciences)

The University of Western Ontario
London, Ontario, Canada
2014-2016 M.Sc. (Medical Biophysics)

Honours and Awards: Queen Elizabeth II Aiming for the Top Scholarship
2009-2014

The University of Western Ontario Gold Medal
Applied Mathematics
2014

Province of Ontario Graduate Scholarship
2014-2016

Benjamin Zweifach Student Travel Award
The Microcirculatory Society
2016

Related Work Experience Teaching Assistant
The University of Western Ontario
Biophysics of Transport Systems 3501F
2015

Publications

Refereed Articles:

Al Tarhuni M, Goldman D, Jackson DN. Comprehensive in situ analysis of arteriolar network geometry and topology in rat gluteus maximus muscle. *Microcirculation*. 2016.

De Silva, A., Spencer, C. Ho, K.C., **Al Tarhuni, M.**, Go, C., Houde, M., De Solla, S., Lavoie, R., King, L., Muir, D., Fair, P., Wells, R., Bossart, G. Perfluorophosphinates in northern pike (*Esox lucius*), double-crested cormorants (*Phalacrocorax auritus*),

and bottlenose dolphins (*Tursiops truncatus*) in relation to other perfluoroalkyl acids. *Environmental Science & Technology*. (Accepted June 2016).

Al Tarhuni, M., Jackson, D. N., & Goldman, D. Comprehensive Hemodynamic Analysis of Arteriolar Networks in the Rat Gluteus Maximus Muscle. (In preparation - will be submitted Sep. 2016).

Neidert, L. E., **Al-Tarhuni, M.**, Goldman, D., Kluess, H. A., & Jackson, D. N. Endogenous dipeptidyl-peptidase IV modulates skeletal muscle arteriolar diameter in rats. (In preparation – will be submitted Sep. 2016).

Refereed Conference Abstracts:

Al Tarhuni, M., Goldman, D., & Jackson, D. N. (2016). Geometric and Topological Analysis of Arteriolar Networks in the Rat Gluteus Maximus Muscle: One Network to Rule Them All?. *The FASEB Journal*, 30(1 Supplement), 947-7.

Al Tarhuni, M., Jackson, D. N., & Goldman, D. (2016). Comprehensive Hemodynamic Analysis of Arteriolar Networks in the Rat Gluteus Maximus Muscle. *The FASEB Journal*, 30(1 Supplement), 947-9.

Neidert, L. E., **Al-Tarhuni, M.**, Goldman, D., Kluess, H. A., & Jackson, D. N. (2016). Endogenous dipeptidyl-peptidase IV modulates skeletal muscle arteriolar diameter in rats. *The FASEB Journal*, 30(1 Supplement), 946-3.